

LSST

TECHNICAL REPORT

NO. 2006 - 2

ISSN 1880 - 327X

**^{155}Gd , ^{166}Er and ^{237}Np Mössbauer Spectroscopic Studies
on the Structure and Chemical Bonding in Lanthanide
and Actinide Compounds**

Junhu Wang

March 1, 2007



**SCHOOL OF LIFE SYSTEM SCIENCE AND TECHNOLOGY
INSTITUTE FOR ADVANCED STUDIES IN ARTIFICIAL INTELLIGENCE**

CHUKYO UNIVERSITY

101 TOKODACHI, KAIZU-CHO,
TOYOTA, 470-0393, JAPAN
PHONE: +81-565-46-1211 ● FAX: +81-565-46-1299

**^{155}Gd , ^{166}Er and ^{237}Np Mössbauer Spectroscopic Studies
on the Structure and Chemical Bonding in Lanthanide
and Actinide Compounds**

Junhu Wang

March 1, 2007

Abstract

Making clear the structure and chemical bonding feature in *f*-block element compounds is not only important for the basic areas but also for the applied areas of lanthanide (Ln) and actinide (An) science. Mössbauer spectroscopy (MBS) – the nuclear gamma resonant spectroscopy – is a powerful tool for investigating the structure and chemical bonding feature in various materials. The electronic state of target atom is available to be directly reflected in its Mössbauer (MB) spectrum. The MB effect has been confirmed to 14 elements to Ln and 6 elements to An, however, only ^{151}Eu MBS is comparatively applied up to now. Though valuable information is also available to be obtained from MBS of the other *f*-block elements, their MB spectrum measurements are more difficult because of the preparation of MB source by oneself, keeping the radiation source and absorber (sample) at near helium temperature. On one hand, we selected three such MB elements and performed a systematic investigation on the structure and chemical bonding in various materials containing Gd or Er element by using ^{155}Gd and ^{166}Er MBS in connection with powder and/or single-crystal X-ray diffraction method. On the other hand, in relation to the nuclear waste management, ^{237}Np MB spectroscopic studies on the structure and chemical bonding in various materials containing radioactive ^{237}Np element were also conducted. Based on these investigations, differences on the structure and chemical bonding feature in *f*-block element compounds were discussed and much precious results were deduced. In this technical report, the research process and some results are reviewed.

Keywords: *f*-block element; ^{155}Gd , ^{166}Er and ^{237}Np Mössbauer spectroscopy; lanthanide compound; actinide compound; crystal structure; chemical bonding;

^{155}Gd , ^{166}Er および ^{237}Np メスバウアー分光法によるガドリニウム、 エルビウムおよびネプツニウム化合物の配位構造と化学結合の研究

王 軍虎

中京大学生命システム工学部
(2007年4月から中国科学院大連化学物理研究所)

2007年3月1日

要旨

f-ブロック元素化合物の化学結合および配位構造を解明することはランタノイドおよびアクチノイド科学の基礎分野だけでなく応用面からも重要である。メスバウアー分光法は原子核のgamma線に対する無反跳共鳴吸収現象を利用しており、メスバウアー核種の電子状態についての知見を得ることができ、化学結合、配位構造および各種触媒機能材料のIn-situ状態等に関する多くの情報を得ることができる。*f*-ブロック元素のメスバウアー効果についてランタノイドは 14 元素、アクチノイドは 6 元素で観測されるが、 ^{151}Eu のみ多くの研究が行われている。しかしながら測定には線源を自作しなければならなかったり、液体ヘリウム温度近くに冷却しなければならなかったりと困難は伴うものの、有用な化学的な情報が期待できる元素が多くある。本研究ではそのようなメスバウアー元素に注目し、 ^{155}Gd , ^{166}Er および ^{237}Np メスバウアー分光法を用いて種々のガドリニウム、エルビウムおよびネプツニウム化合物を研究し、*f*-ブロック元素化合物の化学結合および構造に関してたくさん貴重な知見を得た。ここで本研究の過程およびいくつかの研究結果をまとめて紹介する。

キーワード: *f*-ブロック元素; ^{155}Gd , ^{166}Er および ^{237}Np メスバウアー分光法; ランタノイド化合物; アクチノイド化合物; 配位構造; 化学結合

从¹⁵⁵Gd, ¹⁶⁶Er及²³⁷Np穆斯谱中获得的镧系和锆系元素化合物的结构和成键信息

王军虎

日本中京大学生命系统工学部

(从 2007 年 4 月开始: 中国科学院大连化学物理研究所)

2007 年 3 月 1 日

摘要

不论从基础科学还是从实际应用的角度来看, 研究和解明镧系和锆系元素化合物材料的结构和化学成键的机理都有很重要的意义。穆斯谱学是通过观测原子核对 γ 线的共鸣吸收现象而研究核外电子举动的科学, 在许多化学领域, 如物质结构, 化学成键, 催化反应及催化剂功能材料的原位状态分析等方面已有广泛地应用。自 1958 年穆斯堡尔效应发现以来, 镧系元素有 14 种, 锆系有 6 种它们的穆斯谱观测法已被确立及报导, 可目前仅有¹⁵¹Eu穆斯谱学在物质材料研究中有较广泛地应用。造成这种状况的原因主要被认为是镧系和锆系的其它的穆斯堡尔元素的谱图观测与¹⁵¹Eu及最常见的⁵⁷Fe和¹¹⁹Sn相比有一定的难度, 如放射源必须自己制作, 必须在接近液氦的低温下方可测量等。可是, 从这样的元素的穆斯谱上同样可得到许多用其它谱学法难以得到的独特信息。作者着眼于这类穆斯堡尔元素, 制作了优质的穆斯谱单线放射源, 在世界上首次系统开展了¹⁵⁵Gd和¹⁶⁶Er穆斯谱学在各种钷和铈配位络合物材料的结构和化学成键中的应用研究。同时, 与日本原子力研究所合作, 从放射性废物处理及无机结构化学的观点出发, 用²³⁷Np穆斯谱学结合差热分析, 磁性测量及X衍射表征等对Np(VI)配位络合物也进行了系统研究。根据以上研究结果, 作者系统对比考察了镧系和锆系元素化合物材料的结构异同及 4*f*和 5*f*轨道在化学成键中所起的不同作用。本技术报告将对上述的研究过程及其代表性的一些研究结果做一概述。

关键词: ¹⁵⁵Gd, ¹⁶⁶Er和²³⁷Np穆斯谱学; 镧系元素化合物; 锆系元素化合物; 配为结构; 化学成键机理; 4*f*和 5*f*轨道

^{155}Gd , ^{166}Er and ^{237}Np Mössbauer Spectroscopic Studies on the Structure and Chemical Bonding in Lanthanide and Actinide Compounds

Junhu Wang

School of Life System Science and Technology, Chukyo University, 101 Tokodachi, Kaizu, Toyota, 470-0393 Japan (From April, 2007: Dalian Institute of Chemical Physics, Chinese Academy of Sciences, 457 Zhongshan Road, Dalian, 116023 China)

1. Introduction

Materials containing lanthanide (Ln) and/or actinide (An) elements have been widely applied in advanced functional material, nuclear fuel and nuclear waste management, due to their unique physico-chemical properties. However, the roles of $4f$ and $5f$ orbits in chemical bonding are still unclear. Though electronic structure calculation methods are used to make clear the roles of $4f$ and $5f$ orbits in chemical bonding and some valuable results have been reported so far, the evidences directly observed by experiment are still not many. Therefore, making clear the coordination structure and chemical bonding feature in the f -block element compounds is not only important in the basic areas but also in the applied areas of Ln and An science.

On one hand, the $4f$ orbit of Ln is not traditionally considered to be a participant in chemical bonding. Recent years, mainly based on the electronic structure calculations, participation of $4f$ and $5d$ orbits in covalent bonding are evolved [1,2]. On this viewpoint, more detail investigation is needed, especially sufficient evidence directly obtained from an experimental basis. On the other hand, the $5f$, $6s$, $6p$ and $6d$ orbits of An are considered to participant in chemical bonding. This leads to (a) a bigger range of oxidation states than with Ln; (b) a greater tendency to covalent formation (but maybe involving $6d$ rather than $5f$) in ions like AnO_2^+ and AnO_2^{2+} (most notably the uranyl ion, UO_2^{2+} and the neptunyl ion, NpO_2^+) [1]. The role of each orbit involved in chemical bonding of An needs to be investigated furthermore. A comparative study of Ln and An is a good way for understanding their coordination structure, chemical bonding feature, and fundamental physico-chemical property, and even for developing novel functional materials as luminous material, nuclear material.

Mössbauer (hereafter called MB) effect refers to the resonant and recoil-free emission & absorption of γ rays by atomic nuclei bound in a solid form [3]. Nearly fifty years ago, whilst working on his doctoral thesis under Professor Maier-Leibnitz in Heidelberg, Rudolf L. Mössbauer made this important discovery. Since the states of electrons around a MB atomic nuclei are available to be directly reflected in the hyperfine structure of its MB spectrum, Mössbauer spectroscopy (here after called MBS) or the nuclear gamma resonant spectroscopy has become a powerful tool to investigate the coordination structure and chemical bonding feature in various functional materials. The MB effect has been confirmed to have about 100 nuclear transitions in some 80 nuclides in nearly fifty elements. There are 14 elements to Ln and 6 elements to An that the MB effect is available to be observed as shown in **Figure 1**, however, only ^{151}Eu MBS is comparatively applied. Though valuable information can be also obtained from MBS of the other f -block elements, their MB spectrum

measurements are more difficult because of MB source preparation, keeping the source and absorber (sample) at near helium low temperature.

1																	18
H																	He
2												13	14	15	16	17	
Li	Be											B	C	N	O	F	Ne
3												13	14	15	16	17	
Na	Mg											Al	Si	P	S	Cl	Ar
4												13	14	15	16	17	
K	Ca	Sc	Ti	V	Cr	Mn	Fe	Co	Ni	Cu	Zn	Ga	Ge	As	Se	Br	Kr
5												13	14	15	16	17	
Rb	Sr	Y	Zr	Nb	Mo	Tc	Ru	Rh	Pd	Ag	Cd	In	Sn	Sb	Te	I	Xe
6												13	14	15	16	17	
Cs	Ba	*	Hf	Ta	W	Re	Os	Ir	Pt	Au	Hg	Tl	Pb	Bi	Po	At	Rn
7												13	14	15	16	17	
Fr	Ra	**	Rf	Db	Sg	Bh	Hs	Mt	Uun	Uuu	Uub						

* Ln	La	Ce	Pr	Nd	Pm	Sm	Eu	Gd	Tb	Dy	Ho	Er	Tm	Yb	Lu
** An	Ac	Th	Pa	U	Np	Pu	Am	Cm	Bk	Cf	Es	Fm	Md	No	Lr

Figure 1. Mössbauer elements.

(The elements observed Mössbauer effect so far are shown in pink)

We selected such three MB elements and performed a systematic investigation on various functional materials containing Gd and Er by using ^{155}Gd and ^{166}Er MBS in connection with powder and/or single-crystal X-ray diffraction (XRD) method. At the same time, in relation with nuclear waste management, ^{237}Np MB spectroscopic studies on various materials containing Np were also conducted. Based on a large quantity of experimental results, the differences on the coordination structure and chemical bonding feature in a large number of Ln and An compounds were studied and much precious information were deduced [4]. In this technical report, the research process and some results are reviewed.

2. ^{155}Gd , ^{166}Er and ^{237}Np MBS [5-7]

Generally, three principal hyperfine interactions are available to be observed from MBS. They are monopolar electric interaction, quadrupolar electric interaction and dipolar magnetic interaction. The first one derives from the coupling between the charge distribution of the protons in the nucleus and that of the electrons penetrating the nuclear volume. It leads to the isomer shift, δ . The electronic charge density inside the nuclear volume results from the direct contribution of the *s*-electrons; the *p*, *d* or *f* electrons interact indirectly via a screening effect. The isomer shift provides information on the charge state, the bonding nature, the number and distance of the nearest neighbors, the number of sites containing the resonant atom and so on.

The quadrupole electric interaction is produced by the coupling between the quadrupole moment Q of the nucleus and the non-spherical distribution of the electrical charges (ionic charge on the lattice and contribution of the valence electrons) which induces an electrical field gradient (EFG) at the site of the resonant nucleus. The quadrupole splitting, e^2qQ , provides information on the symmetry of the coordination polyhedron and the valence

electron contribution.

The dipolar magnetic interaction has its origin in the coupling of a magnetic dipole moment, μ , of a spin I nuclear level, with the effective magnetic field, H_{eff} , at the nuclear site. Relaxation phenomena produced by dynamic interactions (spin fluctuations) lead to more or less well resolved spectra, according to the relaxation time, τ . When the relaxation time is very large, if compared with the Larmor precession period, a static hyperfine magnetic field is observed. In a more detailed discussion one would have to distinguish relaxation processes in a paramagnet or in an ordered magnet.

Extensive experimental work has been reported previously and an excellent review has given by Czjzek [5] about ^{155}Gd MBS, which gives information on δ and e^2qQ . No relaxation phenomena have been discussed up to now on ^{155}Gd MBS. ^{237}Np MBS, which has been described in numerous articles and reviews, gives information on δ , e^2qQ , H_{eff} and τ . Among of them, research work is not so many to be reported up to now on ^{166}Er MBS, which gives information on H_{eff} , e^2qQ and τ and the e^2qQ value is available to be obtained only in the case of the existence of the effective magnetic field, H_{eff} .

MB study on coordination compound is mainly on Np. Before our research is reported, no any work has been done on Gd and Er. About experimental techniques, points in common, are that ^{155}Gd , ^{166}Er and ^{237}Np MBS are restricted to low temperature because of the high energy of the gamma rays. That is to say, the radiation source and absorber must be in a cryostat. Furthermore, fine radiation sources for ^{155}Gd and ^{166}Er MBS are only available to be made for oneself. The additional description is separately given as below on the three MBS in short.

A dilute solution of ^{155}Eu diffused into Pd or the compound $^{154}\text{SmPd}_3$ after neutron irradiation is a fine single-line source for ^{155}Gd MBS. Three gamma transitions (60.0, 86.5, 105.3 keV) can be employed for ^{155}Gd MBS. At present, only the 86.5 keV transition is employed extensively since its resulting MB spectrum has the best resolution. Since the change of the mean-square nuclear radius $\Delta\langle r^2 \rangle$ is negative for the 86.5 keV transition of ^{155}Gd , the small δ the large s -electron density at the resonant nucleus position is. The large range of δ values has been observed in the metallic Gd compounds from about -0.2 to nearly 0.9 mm s^{-1} . Since the Q of the 86.5 keV state ($I = 5/2$) is very smaller than that of the ground state ($I = 3/2$), only the ground state splitting is resolved, resulting that the spectra have the appearance of doublets. When ^{155}Gd nuclei are in a site of cubic point symmetry and experience a magnetic field, the MB spectrum is split into 12 lines due to the magnetic hyperfine interaction. There are three groups of 4 lines each since the two g factors are nearly equal for the ground and 86.5 keV states.

The compound $\text{Ho}_{0.4}\text{Y}_{0.6}\text{H}_2$ after neutron irradiation is a useful single-line source for ^{166}Er MBS and gamma transition of 80.6 keV is employed. Since the change of the mean-square nuclear radius $\Delta\langle r^2 \rangle$ is very small for the 80.6 keV transition of ^{166}Er , the δ is not available to be observed. Because the 80.6 keV transition in ^{166}Er is E2 transition, the ground state ($I = 0$) is not split, the 80.6 keV state is split into five equally spaced levels when the magnetic hyperfine interaction is existed, and the five equally spaced levels are further shifted when the quadrupole hyperfine interaction is existed.

Metallic ^{241}Am radioactive isotope is used as the source for ^{237}Np MBS and gamma transition of 59.6 keV is employed. The special feature of ^{237}Np MBS is that the oxidation

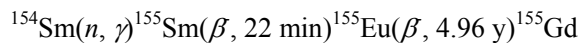
number of Np can be sensitively reflected from the δ value. For the 59.6 keV transition of ^{237}Np , the sign of the mean-square nuclear radius $\Delta\langle r^2 \rangle$ is negative and it is the same with that of the 86.5 keV transition of ^{155}Gd , but the change is very larger. In the case of pure quadrupole hyperfine interaction, the spectrum shows five lines and is symmetric with respect to the central line when the electric field gradient is axial symmetry, it shows three lines when the asymmetry parameter, η is equal to 1. The spectrum, which is symmetrical for pure magnetic splitting, has 16 lines. In the case of non-collinear magnetic and quadrupole hyperfine interactions, the spectrum becomes more complex.

3. Preparation of MB Sources $^{155}\text{EuPd}_3$ and $^{166}\text{Ho}_{0.4}\text{Y}_{0.6}\text{H}_2$

3.1. $^{155}\text{EuPd}_3$ Source for ^{155}Gd MBS [8]

In this study, firstly a fine single-line $^{155}\text{EuPd}_3$ source (about 231 MBq) for ^{155}Gd MBS was prepared by chemical synthesis and neutron irradiation of the compound $^{154}\text{SmPd}_3$. $^{154}\text{SmPd}_3$ was only prepared by the conventional solid state reaction in a H_2 atmosphere at high temperature. According to the previous report, the product was mixed hydrides after the mixture of $^{154}\text{Sm}(\text{HCOO})_3$ and PdH_x was calcined at high temperature in a H_2 atmosphere. However, the product obtained in this study was confirmed as $^{154}\text{SmPd}_3$, not as $^{154}\text{SmPd}_3\text{H}_x$ or $^{154}\text{SmH}_x$ and PdH_x , by the channeling method through the nuclear reaction $^1\text{H}(^{11}\text{B}, \alpha)\alpha\alpha$. In addition, Pd fine particles used to synthesize starting material PdH_x were prepared by a chemical solution process in order to increase the relative reaction area.

Secondly, the prepared $^{154}\text{SmPd}_3$ (about 312.4 mg) pellet was wrapped with Al sheet with 99.99% purity and irradiated by JRR-3M-HR-1 reactor (the flux of neutrons: $6.0 \times 10^{13} \text{ cm}^{-2} \text{ s}^{-1}$) for 67 h in Japan Atomic Energy Research Institute (JAERI, presently the Japan Atomic Energy Agency). After irradiation, the sample was left in JAERI for one month in order to wait for the Pd activity to die. Scheme of the nuclear reaction was shown as the follows:



Finally, the prepared $^{155}\text{EuPd}_3$ source was mounted to an Al holder and again wrapped by Al sheet with 99.99% purity. Araldite adhesive was used in order to mount the source on the holder tightly. Its high performance was proved by observing the ^{155}Gd MB spectra of

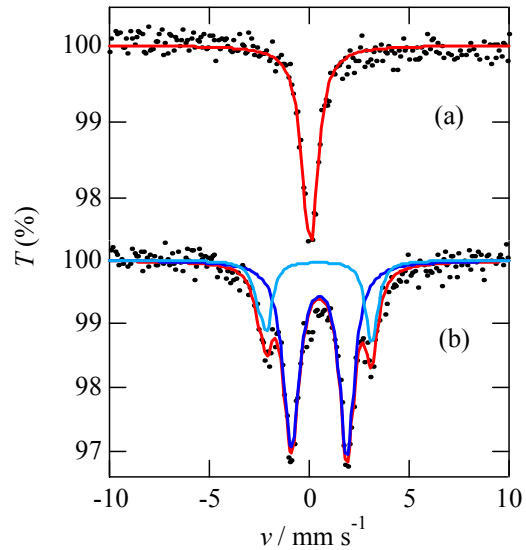


Figure 2. ^{155}Gd Mössbauer spectra of GdPd_3 (a) and cubic Gd_2O_3 (b) at 12 K obtained in this study.

known compounds, GdPd₃ and cubic Gd₂O₃ as shown in **Figure 2**. The GdPd₃ is iso-structural with the source compound, ¹⁵⁴SmPd₃ and its ¹⁵⁵Gd MB spectra were known to show single-line pattern. The cubic Gd₂O₃ have two crystallographically inequivalent Gd³⁺ sites and the population is 3:1, which can be identified clearly by ¹⁵⁵Gd MBS. The obtained results in this study indicate that the newly prepared source is single-line and fine enough to investigate the structural characteristic of materials containing Gd.

3.2. ¹⁶⁶Ho_{0.4}Y_{0.6}H₂ Source for ¹⁶⁶Er MBS [9]

The preparation of the ¹⁶⁶Ho_{0.4}Y_{0.6}H₂ MB source was according to the following procedure: the alloy of Ho_{0.4}Y_{0.6} (about 200 mg) was wrapped in a Ti sheet which acted as oxygen getter and moreover wrapped in a Ta sheet, and then was put into a quartz tube. The quartz tube was connected to a vacuum system containing a manometer and put it into an electronic furnace. After evacuating, the quartz tube was heated to 1273 K for 2 h and then down to 1123 K. Dried hydrogen gas was through the quartz tube by a pressure of 200 Torr. The Ho_{0.4}Y_{0.6} alloy was almost immediately reacted with hydrogen at 1123 K. In order to avoid the formation of trihydrate Ho_{0.4}Y_{0.6}H₃, the quartz tube was cooled rapidly from 1123 K to room temperature by liquid nitrogen. The prepared Ho_{0.4}Y_{0.6}H₂ dihydrate compound was checked by XRD that revealed it had a cubic CaF₂-type structure.

The prepared Ho_{0.4}Y_{0.6}H₂ (about 55 mg) was pelletized into a disc (ϕ10 mm). The disc was wrapped by Al sheets and then irradiated at JAERI with JRR-3M PN-1 (neutron flux of 6.0 × 10¹³ cm⁻²s⁻¹) for 9 min. The obtained ¹⁶⁶Ho_{0.4}Y_{0.6}H₂ (about 1.5 GBq) MB source was evaluated by a standard absorber, ErH₂. ErH₂ was iso-structural with the source compound, Ho_{0.4}Y_{0.6}H₂ and its ¹⁶⁶Er MB spectrum was known to show a narrower single-line pattern (the line-width of 2Γ = 7.7 mm s⁻¹ at 4.2 K). As shown in **Figure 3**, the spectrum of ErH₂ obtained in this study is single-line pattern and has a line-width of 2Γ = 8.0 mm s⁻¹ at 12 K. It indicates the prepared ¹⁶⁶Ho_{0.4}Y_{0.6}H₂ source is fine enough. Since the half life of ¹⁶⁶Ho is short as 26.9 h, a ¹⁶⁶Ho_{0.4}Y_{0.6}H₂ source is only available to be used about 7~10 days for measuring 3~4 samples.

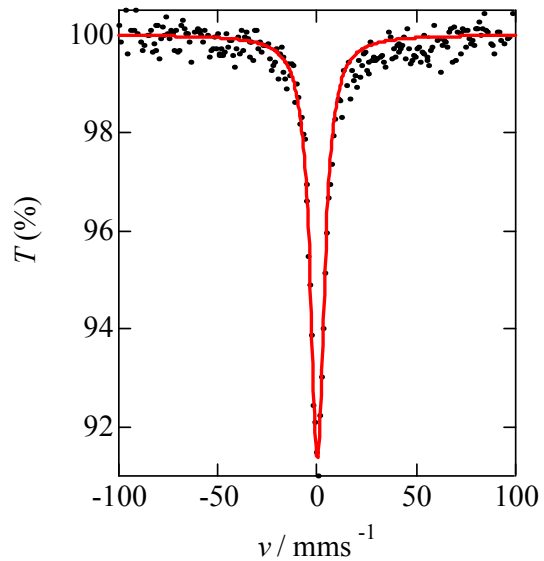


Figure 3. ¹⁶⁶Er Mössbauer spectrum of ErH₂ at 12 K obtained in this study.

4. ¹⁵⁵Gd, ¹⁶⁶Er and ²³⁷Np MB Measurements [8-10]

The ¹⁵⁵Gd and ¹⁶⁶Er MB spectra were measured by using the prepared ¹⁵⁵EuPd₃ and ¹⁶⁶Ho_{0.4}Y_{0.6}H₂ sources on a WissEl MB measuring system consisting of MDU-1200, DFG-1200 and MVT-1000, respectively. The ²³⁷Np MB spectra were measured on the same

model MB system at JAERI by using an assembled metallic ^{241}Am source (about 600 MBq) purchased from Russian. The following points were in common for the three MB measurements. Both of the radiation source and samples were kept at low temperature in a cryostat equipped with a closed-cycle refrigerator. The MB gamma rays (86.5 keV for ^{155}Gd , 80.6 keV for ^{166}Er and 59.6 keV for ^{237}Np) were separately counted with a pure Ge detector. The Doppler velocity was measured with a laser MB velocity calibrator WissEl MVC-450. The absorber thickness was 115 mg Gd cm^{-2} , 200 mg Er cm^{-2} and 120 mg Np cm^{-2} for the ^{155}Gd , ^{166}Er and ^{237}Np MB measurement, respectively. The ordinary MB spectra (no relaxation phenomenon) were computer-fitted by using a sum of the Lorentz approximation. The paramagnetic relaxation ^{166}Er and ^{237}Np MB spectra were analyzed by using the relaxation-fitting procedure based on the Nowik and Wickman model. The value of δ is referred to the radiation source $^{155}\text{EuPd}_3$ at 12 K for ^{155}Gd and NpAl_2 at 4.2 K for ^{237}Np .

5. Crystal Structure of Ln(III)- β -Diketonato Complex (Ln = Gd or Er) [9, 11]

Mainly based on the previous report of ^{151}Eu MB studies, the structure and chemical bonding in Ln(III)- β -diketonato complexes (Ln = Gd or Er) were selected as one of main subject of our investigation. In order to give a more reasonable explanation to their MB results, single-crystal X-ray structural determinations were done to several prepared Ln(III)- β -diketonato complexes. Ten β -diketone ligands and their abbreviations used in this study are shown in **Figure 4**.

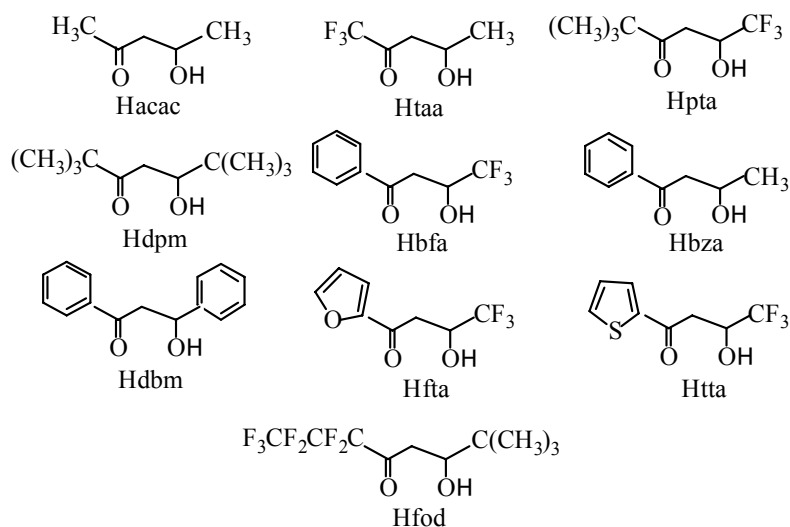


Figure 4. Ten β -diketone ligands and their abbreviations used in this study.

5.1. Material Preparation

Polycrystalline samples of the Ln(III)- β -diketonato complexes (Ln = Gd or Er) were prepared by modifying the previous method except $\text{Gd}(\text{acac})_3 \cdot 3\text{H}_2\text{O}$. $\text{Gd}(\text{acac})_3 \cdot 3\text{H}_2\text{O}$ was purchased from Aldrich Chemical Co. Inc. A typical procedure was particularly described by

preparing the Er(III) dpm complexes. In order to obtain single crystals with reasonable size and good quality for the three-dimensional X-ray structure analysis, numerous attempts were made. As a result, single-crystals of Gd(pta)₃•2H₂O **1**, Gd(bfa)₃•2H₂O **2** and Er(pta)₃•H₂O **3** were obtained by recrystallizing their crude product from n-hexane, respectively. Single-crystals of Er₂(pta)₆ **4** and Er(dpm)₃ **5** were obtained from subliming the crude products under reduced pressure at 423-473 K, respectively. Single-crystals of Er(dpm)₃•H₂O **6** were obtained through keeping the solution dissolving the **5** into n-hexane at 277 K after two days. Compositions of all the polycrystalline samples were decided by the chemical analysis. All the polycrystalline samples were dried in a vacuum desiccator over three days before the chemical analysis and the MB measurement were conducted. The C, H and N chemical analysis were carried out with a Perkin-Elmer Model 2400. Gd and Er contents were determined by the chelatometric titration on the asked samples with H₄edta (ethylenediaminetetraacetic acid) standard solution.

5.2. Crystal Structure Determination

Crystal structures of the six prepared β -diketonato complexes (separately noted **1**, **2**, **3**, **4**, **5**, **6** as above) were determined by three-dimensional X-ray methods. The reflection data were collected on a Rigaku AFC5S diffractometer with the graphite monochromated Mo-K α radiation ($\lambda = 71.069$ pm) at room temperature. The structure for the **5** was solved by a direct method using a SAPI92 program and those for the **1**, **2**, **3**, **4** and **6** were solved by a heavy atom method using a DIRDIFF92 program, and the structures were expanded by using Fourier techniques. All the calculations were performed by using a teXsan crystallographic software package from Molecular Structure Corporation.

The X-ray crystallographic files in CIF for the **3**, **4**, **5** and **6** were deposited as Document No. 75020 at the Office of the Editor of Bull. Chem. Soc. Jpn and also deposited at the CCDC, 12 Union Road, Cambridge CB21EZ, UK. And their copies can be obtained on request, free of charge, by quoting the deposition numbers 177648-177651. The X-ray crystallographic files in CIF for the **1** and **2** were also deposited at the CCDC, 12 Union Road, Cambridge CB21EZ, UK and their copies can also be obtained on request, free of charge, by quoting the deposition numbers 181237-181238. We are planning to publish their details, too.

5.3. Gd(III) and Er(III) pta Complexes

For Gd and Er pta complex, crystal structures of Gd(pta)₃•2H₂O **1**, Er(pta)₃•H₂O **3** and Er₂(pta)₆ **4** were successfully determined. The Crystal structure of Ln pta complex has not yet been found to be reported. This report should be the first time. The results obtained from infrared spectroscopic studies indicate that anhydrous and monohydrate species are possible for the Ln pta complex. The crystal structures for **1**, **3** and **4** determined in this study indicate that the Ln pta complex crystallizes not only in anhydrous and monohydrate structures but also in dihydrate structure.

Figures 5a, 5b, 5c show the structures for **1**, **3** and **4**, respectively. The Gd(III) ion in **1** is eight-coordinated with three bidentate pta ligands and two water molecules. However, the Er(III) ion in **3** is seven-coordinated with three bidentate pta ligands and one water molecule.

Moreover, it is interesting that **4** has a dimeric structure as being observed in the Ln dpm complexes, $\text{Ln}_2(\text{dpm})_6$ (Ln = La-Dy); each Er(III) ion is seven-coordinate and one of the chelating oxygen atoms of the pta ligand bridges Er(pta)₃ fragments, serving as the seventh ligand atom.

The coordination polyhedron around Gd(III) in **1** is a distorted square antiprism. This configuration has also been found in some other reported crystal structures as $\text{Gd}(\text{acac})_3 \cdot 3\text{H}_2\text{O}$ and $\text{Eu}(\text{tta})_3 \cdot 2\text{H}_2\text{O}$. The coordination polyhedron around Er(III) in **3** is a slightly distorted monocapped trigonal prism as being commonly found in many monohydrate Ln β -diketonato complexes. The coordination polyhedron around each Er(III) in **4** is also a slightly distorted monocapped trigonal prism.

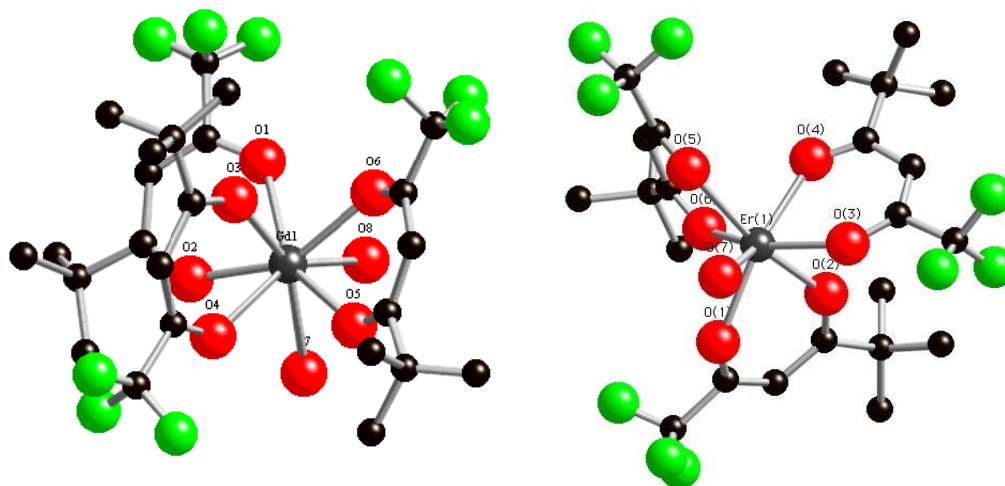


Figure 5a, 5b. The molecule structures of $\text{Gd}(\text{pta})_3 \cdot 2\text{H}_2\text{O}$ **1** (left) and $\text{Er}(\text{pta})_3 \cdot \text{H}_2\text{O}$ **3** (right).

The mean bond length Gd-O (244 pm) for **1** is obviously longer than the mean bond length Er-O (227 pm) for **3** and (229 pm) for **4**. However, the mean bond angle O-Gd-O (71.4°) for **1** is clearly smaller than the mean bond angles O-Er-O (75.2°) for **3** and (74.7°) for **4** in the same pta chelate rings. The shortest Gd(III)-Gd(III) distance in **1** is 610.4 pm. The shortest Er(III)-Er(III) distance in **3** is 587 pm, being shorter than that of **1**. The shortest Er(III)-Er(III) distance in **4** is 382 pm, being the intermolecular Er1-Er2 distance and clearly shorter than that of **1** and **3**.

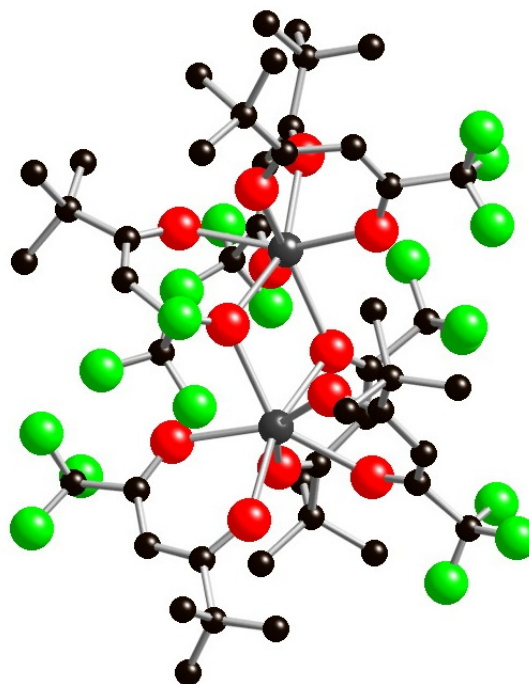


Figure 5c. The molecule structure of $\text{Er}_2(\text{pta})_6$ **4**.

5.4. Gd(III) bfa Complex

For Gd and Er bfa complexes, only the crystal structure of $\text{Gd}(\text{bfa})_3 \cdot 2\text{H}_2\text{O}$ **2** was successfully determined in this study. This is also the first report on the crystal structure of the Ln pta complex. The structure of **2** as shown in **Figure 6** is similar to that of **1**. That is to say, the Gd(III) ion in **2** is eight-coordinated with three bidentate bfa ligands and two water molecules and the coordination polyhedron around Gd(III) is a distorted square antiprism.

Mean bond length Gd-O (245 pm) for **2** is almost similar to that of **1** (244 pm) and is clearly longer than that of $\text{Gd}(\text{acac})_3 \cdot 3\text{H}_2\text{O}$ (237 pm) being reported as the Gd(III) ions coordinating with three bidentate acac ligands and two water molecules. Mean bond angle O-Gd-O (71.3°) for **2** is almost the same with that of **1** (71.4°) in the same chelate rings and is smaller than that of $\text{Gd}(\text{acac})_3 \cdot 3\text{H}_2\text{O}$ (72.0°). The shortest Gd(III)-Gd(III) distance in **2** is 609.2 pm, being almost the same with that of **1** (610.4 pm).

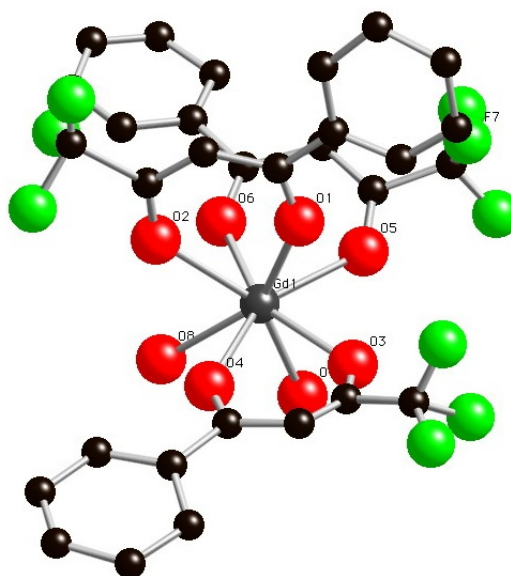


Figure 6. The molecule structure of $\text{Gd}(\text{bfa})_3 \cdot 2\text{H}_2\text{O}$ **2**.

5.5. Er(III) dpm Complex

For Gd and Er dpm complexes, crystal structures of $\text{Er}(\text{dpm})_3$ **5** and $\text{Er}(\text{dpm})_3 \cdot \text{H}_2\text{O}$ **6** were determined in this study. Up to now, three kinds of complexes (nonaqua, monoqua and dimer) have been reported for the Ln dpm complex. The crystal structure of **5** has been reported previously and is confirmed by us in this study. To the Ln β -diketonato complex, this is the only one that the crystal structure of the monomer anhydrous complex has been solved up to now. Other reported structures of the Ln- β -diketonato complexes are hydrates, hydrated dimers and various adducts and the Ln(III) ion in those complexes are seven or eight coordinates. Crystal structures of the monoqua for the Ln dpm complex have been reported for $\text{Eu}(\text{dpm})_3 \cdot \text{H}_2\text{O}$ and $\text{Dy}(\text{dpm})_3 \cdot \text{H}_2\text{O}$. The dimeric structures for the Ln dpm complexes have been known for La-Dy.

For Gd dpm complex, the crystal structures of the monoqua and dimer have been identified in this study. **Figure 7** shows the observed XRD patterns for the prepared Gd dpm complex and the calculated XRD patterns for $\text{Pr}_2(\text{dpm})_6$ based on the reported single-crystal X-ray structural data. It clearly indicates that the prepared Gd dpm complex is iso-structural to $\text{Pr}_2(\text{dpm})_6$ and its chemical formula should be written as $\text{Gd}_2(\text{dpm})_6$. Moreover, the monoqua, $\text{Gd}(\text{dpm})_3 \cdot \text{H}_2\text{O}$, can be obtained by recrystallizing the prepared $\text{Gd}_2(\text{dpm})_6$ sample from 95% methanol. We attempted to determine the crystal structure of the monoqua by three dimensional X-ray analysis, unfortunately, the obtained single-crystals were not good enough for the full measurement. As a result, its crystal system was determined as triclinic and its

lattice parameters were determined as $a = 1402.4(5)$, $b = 1652.4(7)$, $c = 1067.7(2)$ pm, $\alpha = 95.33(3)$, $\beta = 104.25(2)$, $\gamma = 115.07(3)^\circ$. These results indicate that the obtained single-crystal is the monoaqua, $\text{Gd}(\text{dpm})_3 \cdot \text{H}_2\text{O}$ being iso-structural to $\text{Er}(\text{dpm})_3 \cdot \text{H}_2\text{O}$ and the reported

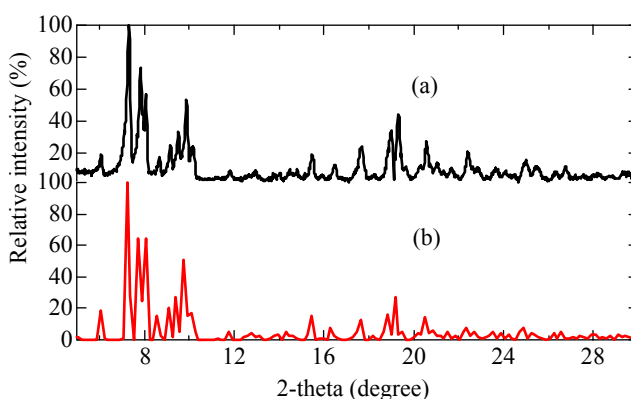


Figure 7. The observed XRD patterns for the prepared Gd(III) dpm complex (a) and the calculated XRD patterns for $\text{Pr}_2(\text{dpm})_6$ based on the reported single-crystal X-ray structural data.

$\text{Dy}(\text{dpm})_3 \cdot \text{H}_2\text{O}$. From the consideration of Ln contraction, it has been suggested that the monoaqua dpm complex could not be formed for the Ln ions

heavier than Dy. Our study, however, indicates that the monoaqua dpm complex is available to be formed for Er, even though the ion radius is smaller than that of Dy.

As reported previously, Er(III) in **5** is coordinated with three bidentate dpm ligands. Interestingly, one of the dpm chelate rings lies in a mirror plane and the other two are symmetry related across this mirror plane. The crystal structure of **6** as shown in **Figure 8** is similar to that of **3** and is iso-structural to the reported $\text{Dy}(\text{dpm})_3 \cdot \text{H}_2\text{O}$. Er(III) in **6** is coordinated with three bidentate dpm ligands and one water molecule. The coordination polyhedron around Er(III) are a trigonal prism in **5** and a slightly distorted monocapped trigonal in **6** as same as being observed in **3** and the reported $\text{Dy}(\text{dpm})_3 \cdot \text{H}_2\text{O}$.

The mean bond length Er-O (223 pm) for **5** is clear shorter than that of seven-coordinated complexes, such as **6** (227.1 pm) and $\text{Dy}(\text{dpm})_3 \cdot \text{H}_2\text{O}$ (229.4 pm) and eight-coordinated complexes, such as **2** (244 pm). The difference 2.3 pm between the mean bond length Er-O of **6** and $\text{Dy}(\text{dpm})_3 \cdot \text{H}_2\text{O}$ compares favorably with the difference of the seven coordinated ion radius of Er (94.5 pm) and Dy (97.0 pm) and is well interpreted by the Ln contraction. The mean bond angle O-Er-O (74.3°) in the same dpm chelate rings for **6** is almost the same with that of **5** (74.1°), however, is slightly larger than that of O-Dy-O (73.6°) for $\text{Dy}(\text{dpm})_3 \cdot \text{H}_2\text{O}$. The shortest Er(III)-Er(III) distance is 998 pm in **5** and 558 pm in **6**.

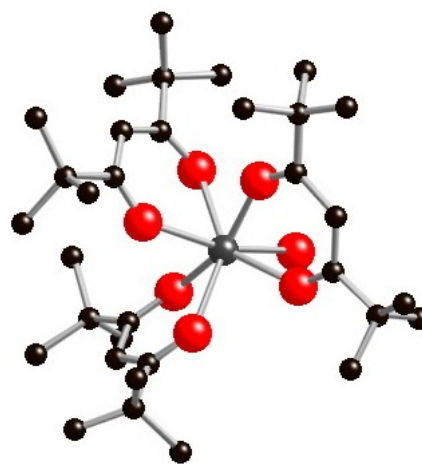


Figure 8. The molecule structure of $\text{Er}(\text{dpm})_3 \cdot \text{H}_2\text{O} **6**.$

6. Information on the Coordination Structure and Chemical Bonding in Gd(III) Metal Complexes [11-20]

Eu and Np compounds, especially their metal complexes, have been studied by using ^{151}Eu and ^{237}Np MBS, respectively. The δ of ^{151}Eu can give valuable information on the bond characteristic as well as the oxidation state of Eu; the δ of ^{237}Np can give information not only on the bond characteristic and the oxidation state of Np but also the coordination number (C.N.) and the mean Np-O bond distance. There is a potentially wide interest in MBS study on the structure and chemical bonding in Gd(III) metal complexes since Gd is located in the middle of the Ln series and can be considered as a representative of Ln in some case.

In our study, a systematic investigation has been finished on the structure and chemical bonding in some Gd(III) metal complexes by ^{155}Gd MBS. The subject of our investigation is various kinds of Gd(III) complexes having different C.N. and different ratios of coordinating oxygen to nitrogen atoms, including β -diketonato complex, cyano-bridged complex, edta complex, terpyridine (terpy) complex and phthalocyanine (H_2Pc) complex. The results indicate a tendency that the δ value decreases with the increase in the C.N. and the number of the nitrogen atoms coordinating to Gd, showing that the Gd-O and/or Gd-N bonds for the investigated Gd(III) metal complexes have a small covalent contribution which is possible to be deduced from the oxygen and/or nitrogen atoms of the ligands donating electrons to $6s$, $5d$ and $4f$ orbitals of Gd.

Figure 9 shows some ^{155}Gd MB spectra for some Gd(III) metal complexes at 12 K. The ^{155}Gd MB parameters and configuration around Gd(III) are listed in **Table 1**. For a comparison, the data of Gd_2O_3 (cubic and monoclinic), GdF_3 and pyrochlore-type $\text{Gd}_2\text{Zr}_2\text{O}_7$ are also listed in **Table 1**. The eight-, nine- and ten-coordinated Gd complexes of N,N' -dimethylformamide (DMF), tetraethylene glycol (EO4), pentaethylene glycol (EO5) and 4,4'-bipyridine N,N' -dioxide (dpdo) are also listed in **Table 1**. All of the ^{155}Gd MB results are obtained in our study. All of the ^{155}Gd MB spectra are typical patterns of electric quadrupole interactions for ^{155}Gd nucleus and the degree of quadrupole splitting are clearly different. The results for Gd_2O_3 and GdF_3 reported here are generally in good agreement with those reported previously.

As described above, δ is a measure of the s -electron density at the MB nucleus and can be influenced by the local structure around the MB nucleus. The definition of δ can be described as below:

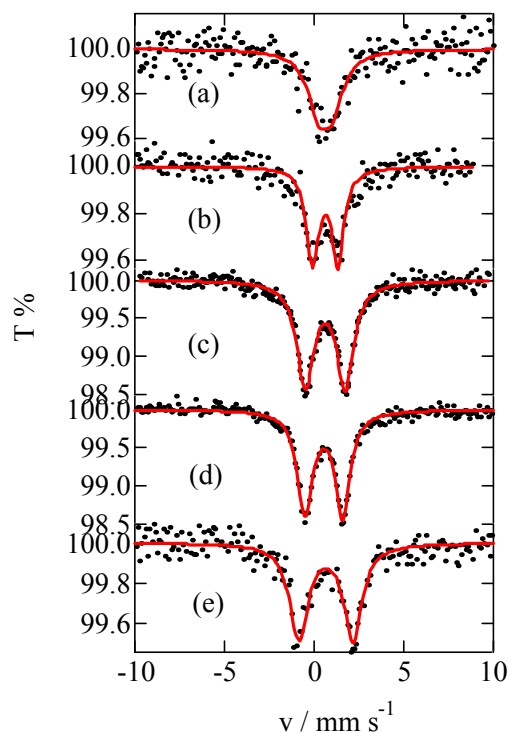


Figure 9. ^{155}Gd Mössbauer spectra for some Gd(III) metal complexes at 12 K. (a) $\text{Gd}(\text{pta})_3 \cdot 2\text{H}_2\text{O}$, (b) $\text{Gd}(\text{bfa})_3 \cdot 2\text{H}_2\text{O}$, (c) $\text{NaGd}(\text{edta}) \cdot 8\text{H}_2\text{O}$, (d) $\text{KGd}[\text{Fe}(\text{CN})_6] \cdot 3\text{H}_2\text{O}$ and (e) $\text{Gd}(\text{dpm})_3$.

Table 1. ^{155}Gd Mössbauer parameters at 12 K and the coordination configuration around Gd(III) for some Gd(III) compounds.

Code	Complex	δ^1 mm s^{-1}	e^2qQ mm s^{-1}	$2I$ mm s^{-1}	Coordination configuration
1	GdF ₃	0.67	6.25	0.92	GdF ₉
2	Gd(η^2 -NO ₃) ₂ (η^1 -NO ₃)(EO4)	0.68	3.53	1.19	GdO ₁₀
3	Gd(η^2 -NO ₃) ₂ (EO5) (NO ₃)	0.65	4.34	1.18	GdO ₁₀
4	Gd(EO5) (H ₂ O) ₃ (ClO ₄) ₃	0.67	3.37	1.13	GdO ₉
5	Gd(NO ₃) ₆ (μ -dpdo) ₃ ·2CH ₂ Cl ₂	0.67	2.78	1.23	GdO ₉
6	NaGd(edta)·8H ₂ O	0.62	4.72	1.10	GdN ₂ O ₇
7	NH ₄ Gd(edta)·6H ₂ O	0.61	3.62	1.35	GdN ₂ O ₆
8	Gd(bza) ₃ ·2H ₂ O	0.64	4.43	1.11	GdO ₈
9	Gd(bfa) ₃ ·2H ₂ O	0.63	3.09	1.28	GdO ₈
10	Gd(pta) ₃ ·2H ₂ O	0.61	1.67	1.45	GdO ₈
11	Gd(tta) ₃ ·2H ₂ O	0.60	7.26	1.23	GdO ₈
12	Gd(taa) ₃ ·3H ₂ O	0.58	4.47	1.27	GdO ₈
13	Gd(acac) ₃ ·3H ₂ O	0.57	5.64	1.38	GdO ₈
14	Gd(fta) ₃ ·3H ₂ O	0.55	7.56	1.21	GdO ₈
15	Gd(fod) ₃ ·H ₂ O	0.55	2.52	1.44	GdO ₈
16	Gd ₂ Zr ₂ O ₇	0.55	8.49	2.15	GdO ₈
17	Gd(dmfa) ₄ (H ₂ O) ₃ (μ -CN) ₃ Fe(CN) ₅	0.66	3.40	1.02	GdNO ₇
18	GdCr(CN) ₆ ·4H ₂ O	0.61	4.30	0.93	GdN ₆ O ₂
19	GdFe(CN) ₆ ·4H ₂ O	0.61	4.07	0.90	GdN ₆ O ₂
20	GdCo(CN) ₆ ·4H ₂ O	0.60	4.12	0.87	GdN ₆ O ₂
21	KGdRu(CN) ₆ ·3H ₂ O	0.60	4.81	1.01	GdN ₆ O ₂
22	KGdFe(CN) ₆ ·3H ₂ O	0.59	4.68	1.04	GdN ₆ O ₂
23	Gd(dpm) ₃	0.65	6.49	1.15	GdO ₇
24	Gd(dbm) ₃ ·H ₂ O	0.60	6.44	1.46	GdO ₇
25	Gd ₂ O ₃ (monoclinic)	0.45 0.46 0.49	5.36 2.78 0.49		GdO ₇ GdO ₇ GdO ₇
26	Gd ₂ O ₃ (cubic)	0.51 0.50	5.53 10.85	0.92 0.70	GdO ₆ GdO ₆
27	GdPc ₂	0.41	3.65	0.64	GdN ₈
28	Gd(terpy) ₃ (ClO ₄) ₃	0.40	1.55	1.55	GdN ₉

(1) Relative to the $^{155}\text{EuPd}_3$ source; Error δ : 0.02 mm s⁻¹; e^2qQ and $2I$: 0.05 mm s⁻¹.

$$\delta = (4/5)\pi Ze^2(\Delta R/R)R^2\{|\psi(o)|_A^2 - |\psi(o)|_S^2\}$$

Here, Z : atomic number; e : elementary electric charge; R : nuclear radius; $|\psi(o)|_A^2$ and

$|\psi(o)|^2_s$: total electron density at the nuclear position of the MB atom in the absorber and radiation source, respectively. The variation in δ for the investigated Gd(III) metal complexes ($0.40 \sim 0.65 \text{ mm s}^{-1}$) are smaller than that for the reported Gd intermetallic compounds ($-0.2 \sim 0.9 \text{ mm s}^{-1}$). However, comparing the δ values of the β -diketonato complexes with the DMF, EO4, EO5, dpdo, edta, CN, terpy and Pc complexes, a tendency shows that the δ values decrease with an increase in the C.N. and the nitrogen atoms coordinating to Gd(III) can be found (see

Figure 10), i.e., $\text{GdO}_{10} \approx \text{GdO}_9 > \text{GdN}_2\text{O}_7 \geq \text{GdO}_8 \approx \text{GdN}_6\text{O}_2 \geq \text{GdO}_7 > \text{GdO}_6 > \text{GdN}_8 \approx \text{GdN}_9$. This indicates that the s -electron density at the MB nucleus is larger as the C.N. decreases and as the coordinating atoms change from oxygen to nitrogen.

Furthermore, all of the δ values fall down between that of cubic Gd_2O_3 and GdF_3 except for the terpy (GdN_8) and Pc (GdN_9) complexes. It means that there is a greater s -electron density at Gd nucleus in each of the investigated Gd(III) metal complexes than in GdF_3 due to $\Delta R/R < 0$ for ^{155}Gd . In the terpy (GdN_8) and Pc (GdN_9) complexes, the s -electron density at Gd nucleus is even greater than in cubic Gd_2O_3 . These results are consistent with those of the ^{151}Eu MB spectroscopic studies on some Eu(III) metal complexes. In the case of ^{151}Eu , $\Delta R/R > 0$, having a positive value, the δ values of the Eu(III)- β -diketonato complexes ($+0.15 \sim +0.56 \text{ mm s}^{-1}$), such as $\text{Eu}(\text{acac})_3 \cdot \text{H}_2\text{O}$, $\text{Eu}(\text{tta})_3 \cdot 2\text{H}_2\text{O}$ and $\text{Eu}(\text{dpm})_3$, also fall down between those of EuF_3 (0 mm s^{-1}) and the cubic Eu_2O_3 ($+1.01 \text{ mm s}^{-1}$). This has been concluded due to small covalent contribution in the Eu(III)- β -diketonato complexes since EuF_3 can be considered as a purely ionic compound. The same should be applied on the Gd(III)- β -diketonato complexes since the nature of the chemical bonding in GdF_3 can also be considered to be closest to purely ionic. Thus, the Gd-F bond in GdF_3 is available to be assumed to be free of covalent contribution. The difference in δ values for cubic Gd_2O_3 and GdF_3 should be considered as the difference in the degree of covalent contribution in their chemical bonding. The tendency of δ observed in this study should indicate that a small covalent contribution exists in the Gd-O and Gd-N bonds of the investigated Gd(III) metal complexes. The decrease in δ value means the increase of covalent contribution in the Gd-O and Gd-N bonds of the investigated Gd(III) metal complexes.

In general, there are two possibilities being able to cause the decrease of δ value for

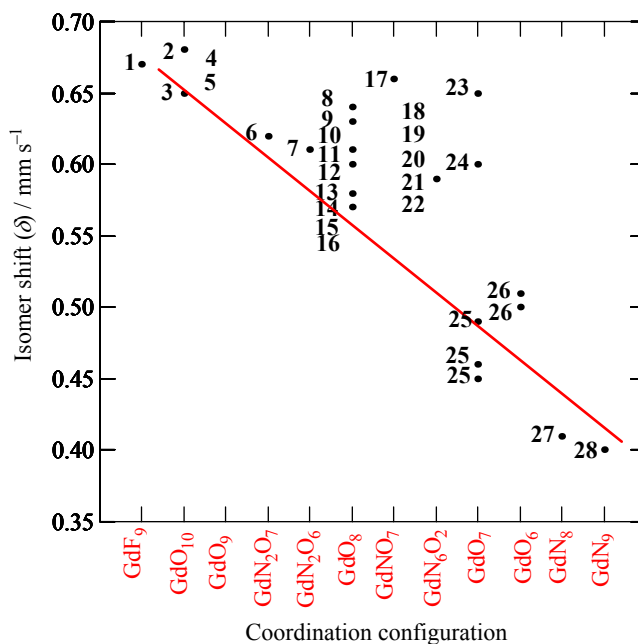


Figure 10. Plot of ^{155}Gd Mössbauer isomer shift (δ) against coordination configuration around the Gd(III) ion in some Gd compounds.

¹⁵⁵Gd: (a) increase electron density of the 6s orbit; (b) decrease of electron density of the 5d and/or 4f orbit, resulting as the decrease of the shielding effect and then increasing s-electron density at the Gd nucleus. Since the covalent contribution in the Gd-O and Gd-N bonds is probably through oxygen and/or nitrogen atoms of ligand group donating electrons to 5d, 4f and 6s (6p) orbits of Gd(III), it is adaptable that the decrease of the δ value is due to the resultant result of the above two possibilities. As mentioned above, the electronic structure calculations have indicated that 5d and 4f orbits participate in the covalent bonding in Ln compounds. Here, ¹⁵⁵Gd MB study indicates that the covalent bonding in Ln compounds is not only possible to be related to their 5d and 4f orbits but also their 6s (6p) orbits.

The electric quadrupole coupling constant, e^2qQ , give a direct measure of the magnitude of the electric field gradient (EFG) at the MB nucleus. The EFG is often produced by charges at greater distance (the lattice EFG) and by valence electrons (the valence EFG). In the case of ¹⁵⁵Gd, the lattice EFG would be dominant in most situations since Gd(III) (4f⁷) has the high symmetric valence electron distribution. Thus, the e^2qQ value is sensitive to the change of the symmetry of the local structure around Gd(III). The e^2qQ values of the investigated Gd(III) metal complexes spread out from 1.67 to 7.56 mm s⁻¹. It should be considered to reflect well the difference in the symmetry of the coordination polyhedron around Gd(III) in these Gd(III) metal complexes. On the other hand, there is a trend that e^2qQ values of the seven-coordinated complexes, such as Gd₂(dpm)₆ and Gd(dbm)₃•H₂O, are larger than that of the eight-coordinated complexes, such as Gd(pta)₃•2H₂O **1** and Gd(bfa)₃•2H₂O **2**. This can be also observed from the Er(III) metal complexes as described in the next section. It is reasonable since the local symmetry around Gd(III) is higher for a square antiprism than that for a monocapped trigonal prism. Gd(fod)₃•H₂O having the smaller e^2qQ value could be considered to have an eight-coordinated dimeric hydrate structure as same as that of the reported Pr₂(fod)₆•2H₂O. The line-width (2I) for the investigated Gd(III) metal complexes range from 1.11 to 1.46 mm s⁻¹. This is broader than that of the ordinary Gd compounds, such as GdPd₃ (0.89 mm s⁻¹) obtained in this study.

7. Paramagnetic Relaxation MB Spectra of ¹⁶⁶Er [9, 19]

MB effect of the 80.6 keV transition in ¹⁶⁶Er has been effectively applied to investigate the structural and magnetic properties of Er containing alloys and intermetallic compounds, but ¹⁶⁶Er MB spectra of the ordinary paramagnetic erbium compounds are scarcely observed, especially the paramagnetic Er(III) metal complexes. An attempt applying the ¹⁶⁶Er MBS for investigating the structural chemistry of various paramagnetic Er compounds, especially various functional paramagnetic Er(III) metal complexes, has been done in our study.

As a preliminary experiment of ¹⁶⁶Er MB spectroscopic study on the structural chemistry of Er(III) metal complexes, ¹⁶⁶Er MB spectra for Er(III) formate, acetate, oxalate and cyano-bridged complexes were firstly observed as shown in **Figure 11**. A wide variety in shape from five line absorption to broad absorption spectrum was observed. It is clearly different from the shapes of the ¹⁶⁶Er MB spectra for Er(HCOO)₃•2H₂O and Er(HCOO)₃. This is considered to be mainly caused by the different paramagnetic τ . So far there were a few studies on the paramagnetic relaxation phenomenon observed in ¹⁶⁶Er MBS, it is probably because the paramagnetic relaxation results a complex shape of the MB spectrum which is

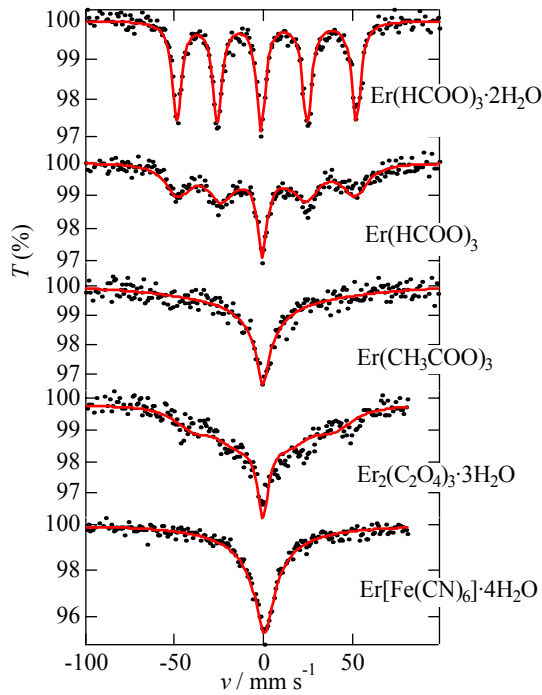


Figure 11. ^{166}Er Mössbauer spectra for some paramagnetic Er(III) metal complexes at 12 K obtained in this study.

difficult to be fitted by Lorentzian lines.

The reason of the paramagnetic relaxation effect is considered to be as follows: the Er(III) ion with electronic configuration $4f^{11}$ has three unpair electrons. All of energy levels of the f orbitals are degenerated into 52 folds in higher symmetrical crystal field. If the Er(III) ion is put into lower symmetrical crystal field, the energy level degenerated into 52 folds will be split into several energy sub-states. The energy sub-state of $J = \pm 15/2$ Kramers doublet can become the ground level due to the spin-orbital interaction in some situation. In this modulation, the relaxation phenomenon can be taken place between the upper spin $+15/2$ and the down spin $-15/2$.

Figure 12 shows some simulated ^{166}Er MB spectra for several τ with $g\mu H_{\text{eff}} = 22 \text{ mm s}^{-1}$ (610 T), $2\Gamma = 8 \text{ mm s}^{-1}$, $\delta = 0 \text{ mm s}^{-1}$ and $e^2qQ = 0 \text{ mm s}^{-1}$ by a relaxation-fitting procedure based on the Nowik and Wickman model. The Zeeman splitting, Δ is assumed to be zero. The relaxed ^{166}Er MB spectra change sensitively with the change in τ about $\tau = 0.002 \sim 20 \text{ ns}$. It indicates the relaxation-fitting procedure based on the Nowik and Wickman model can be used to evaluate the τ of the relaxed ^{166}Er MB spectrum being comparable with the nuclear Larmor precession.

The paramagnetic relaxation has two mechanisms, lattice-spin relaxation and spin-spin relaxation, and sometimes the spin-spin distance has been suggested to be important to determine τ . Therefore we carried out a systematic study by using various Er(III)- β -diketonato complexes to examine the relation between the spin-spin distance and τ by using ^{166}Er MBS in connection with the results of three dimensional X-ray analysis.

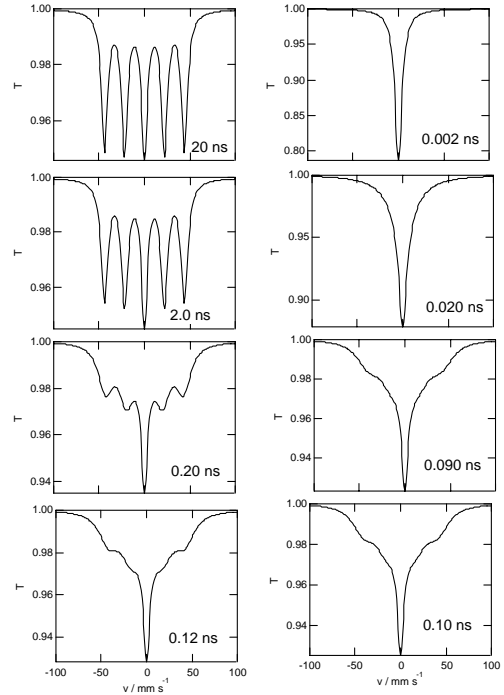


Figure 12. The simulated ^{166}Er Mössbauer spectra for several relaxation times according to the Nowik and Wickman model with $g\mu H_{\text{eff}} = 22 \text{ mm s}^{-1}$ (610 T), $2\Gamma = 8 \text{ mm s}^{-1}$, $\delta = 0 \text{ mm s}^{-1}$ and $e^2qQ = 0 \text{ mm s}^{-1}$. Zeeman Splitting, Δ is assumed to be zero.

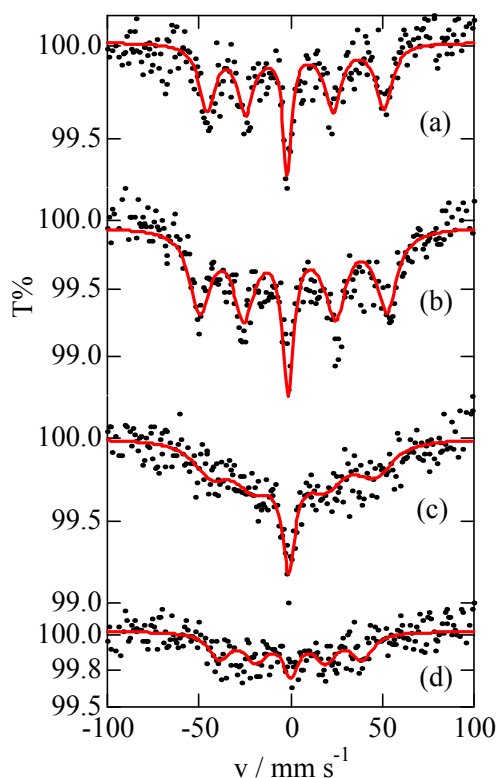


Figure 13a. The ^{166}Er Mössbauer spectra for Er(III)- β -diketonato complexes at 12 K. (a) $\text{Er}(\text{pta})_3 \cdot \text{H}_2\text{O}$ **3**, (b) $\text{Er}(\text{dpm})_3 \cdot \text{H}_2\text{O}$ **6**, (c) $\text{Er}_2(\text{pta})_6$ **4**, and (d) $\text{Er}(\text{dpm})_3$ **5**.

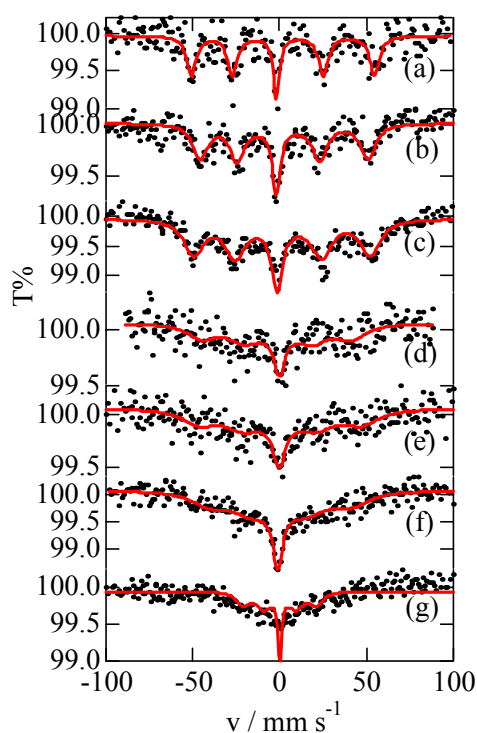


Figure 13b. The ^{166}Er Mössbauer spectra for Er(III)- β -diketonato complexes at 12 K. (a) $\text{Er}(\text{fod})_3 \cdot \text{H}_2\text{O}$, (b) $\text{Er}(\text{pta})_3 \cdot \text{H}_2\text{O}$ **3**, (c) $\text{Er}(\text{dpm})_3 \cdot \text{H}_2\text{O}$ **6**, (d) $\text{Er}(\text{acac})_3 \cdot \text{H}_2\text{O}$, (e) $\text{Er}(\text{bfa})_3 \cdot \text{H}_2\text{O}$, (f) $\text{Er}(\text{taa})_3 \cdot \text{H}_2\text{O}$, (g) $\text{Er}(\text{dbm})_3 \cdot \text{H}_2\text{O}$.

Figures 13a and **13b** show the ^{166}Er MB spectra for the investigated Er(III)- β -diketonato complexes at 12 K. It is clear that the investigated Er(III)- β -diketonato complexes is paramagnetic relaxed ^{166}Er MB spectra. The MB parameters are summarized in **Table 2**. The relative transmission for each complex is less than 1%, being much smaller than that of ionic compounds and alloys having several percent. It indicates that the recoilless even at 12 K. The spectra show a wide variety in absorption shape depending on τ ; a broad single absorption with the short τ and a five-line absorption with the long τ . The estimated τ is spread out from 0.1 to 1 ns.

The estimated τ for the **4** is 0.1 ns, whereas those for the **2** and the **3** are 0.4 and 0.5 ns, respectively. This is the same order to the increase in the shortest Er(III)-Er(III) distances in their crystal structure: 382 pm for the **4**, 558 pm for the **2** and 587 pm for the **3**. Thereby, τ correlates to the intermolecular Er(III)-Er(III) distance. In another word, the spin-spin relaxation is important in the Er(III)- β -diketonato complexes. This is confirmed by examining the MB spectra for the monohydrate complexes (see below). Interestingly, the τ for the **1** is, however, unexpectedly short as 0.4 ns though the shortest Er(III)-Er(III) distance (998 pm) is prominently longer than the other dpm and pta complexes. It will be interpreted as the τ is

dominated by not only the shortest Er(III)-Er(III) distance but also the C.N. Although we could not explain this completely at this stage, the difference in C.N. will lead to the difference in the energy level of the Er(III) ion through a crystal field effect, causing the difference in τ . Indeed, τ for the five Er(III) edta complexes investigated in this study also depends on the C.N. We are planning to publish their details, too.

Table 2 ^{166}Er Mössbauer parameters of the Er(III)- β -diketonato complexes at 12 K.

Complex	e^2qQ mm s^{-1}	$2I$ mm s^{-1}	τ ns	H_{eff} T
Er(fod) ₃ •H ₂ O	6.1	4.1	1.0	711
[Er(pta) ₃ (H ₂ O)]	7.0	5.6	0.5	654
[Er(dpm) ₃ (H ₂ O)]	4.3	8.0 ^{a)}	0.4	690
[Er(dpm) ₃]	0.1	8.0 ^{a)}	0.4	525
[Er(dbm) ₃ (H ₂ O)]	-0.1	8.0 ^{a)}	0.3	294
Er(fta) ₃	-2.4	8.3	0.2	640
Er(acac) ₃ •H ₂ O	-2.7	7.5	0.2	598
Er(tta) ₃ •2H ₂ O	1.8	8.0 ^{a)}	0.2	(316)
[Er ₂ (pta) ₆]	3.6	8.4	0.1	621
Er(bfa) ₃ •H ₂ O	1.0	7.0	0.1	651
Er(taa) ₃ •H ₂ O	2.0	6.8	0.1	582
Er(bza) ₃ •2H ₂ O	-4.0	5.7	0.1	(433)

a). The line-width ($2I$) was fixed at 8.0 mm s⁻¹.

Since τ depends on the C.N., we will focus our interest on the seven-coordinated Er(III)- β -diketonato complexes. As shown already, the C.N. for the Er(III) ions in the two monohydrate **2** and **3** are seven since the water molecule participates in the coordination. This would be safely extended to the other monohydrate Er(III)- β -diketonato complexes though the crystal structure are not known. The XRD pattern indicates that Er(dbm)₃•H₂O is iso-structural to Ho(dbm)₃•H₂O having a monocapped octahedral coordination with C₃ symmetry. Thus, Er(dbm)₃•H₂O can not be included to the following discussion. Indeed, the MB spectrum is clearly different from other seven-coordinated complexes. However, this suggests that the electronic configuration may also play an important role in paramagnetic relaxation.

The values of the τ are widely spread among the monohydrate complexes. The order of the τ is as follows: Er(fod)₃•H₂O > Er(pta)₃•H₂O **3** > Er(dpm)₃•H₂O **2** > Er(acac)₃•H₂O > Er(bfa)₃•H₂O > Er(taa)₃•H₂O. This indicates that the τ depends on the substitute. The substitutes (R₁, R₂) of the β -diketonone (R₁COCH₂COR₂) ligands in the above order is (C₃F₇, t-Bu), (CF₃, t-Bu), (t-Bu, t-Bu), (CH₃, CH₃), (Ph, CF₃) and (CF₃, CF₃). This order is essentially that of the decrease in the bulkiness of the substitutes. Since the Er(III)-Er(III) distance will depend on the size of the substitutes, we can suppose that the τ depends on the intermolecular Er(III)-Er(III) distance as the results. Because we could not know the shortest Er(III)-Er(III) distance by single-crystal X-ray structure determination, we measured the

density of the crystal, expecting the density of the crystal would reflect the intermolecular distance. Such an attempt was, however, unsuccessful. No correlation between the τ and the density could be observed. This would be reasonable since the packing of the molecules in the crystal was not always the same and the substitution of H atom to F atom would result in the increase in density.

Since the MB spectra with longer τ give resolved five-line absorption, we can obtain the value of e^2qQ in good accuracy. Judging from the absorption shape, the values of e^2qQ for Er(fod)₃•H₂O, the **3**, the **2**, and the **1** is considerably reliable. Interestingly, the values for the monohydrate complexes except for Er(dbm)₃•H₂O are obviously larger than that of the anhydrous complex of the **1**. This suggests that there would be some differences in population of the valence orbits between the six- and seven-coordinated complexes. This is reasonable since the local symmetry around the Er(III) ion is higher for trigonal prism than that for monocapped trigonal prism being also confirmed in the seven- and eight-coordinated Gd(III)- β -diketonato complexes. The value of Er(dbm)₃•H₂O is clearly smaller than that of the other monohydrate complexes. This indicates the local symmetry around the Er(III) ion in Er(dbm)₃•H₂O is higher than that of the other monohydrate complexes being in good agreement with the coordination structure.

Concerning with the values of H_{eff} , the most of the values range between 500 and 720 T, being close to that of metallic erbium (742 T). The reliability of the smaller values for Er(tta)₃•2H₂O and Er(bza)₃•2H₂O, figured in parentheses, is rather low. This is resulted from the rapid relaxation and weak absorption.

8. ²³⁷Np MS Spectroscopic Studies on Neptunyl(VI) Compounds [21-24]

Since the gamma ray 59.5 keV MB resonance in ²³⁷Np (5/2 → 5/2) has been found in 1964, various oxides, fluorides, oxyfluorides and polycarboxylic compounds of Np, from III to VII oxidation states, have been investigated by using ²³⁷Np MBS. The δ of ²³⁷Np is spread out from +40 to -80 mm s⁻¹ relative to NpAl₂ at 4.2 K and clearly correlated with the oxidation state of Np. Correlation between the δ and the C.N. of Np has also been found to the Np(VI) compounds. A correlation between the δ and the mean Np-O bond distance has also been reported for the oxygen-coordinated Np(VI) compounds: the δ of ²³⁷Np is increased with the increase of the mean Np-O bond distance. However, about the correlation between the δ and the mean Np-O bond distance, there are some experimental evidences for the six- and eight-coordinated Np(VI) compounds, no data can be found for the seven-coordinated Np(VI) compounds. Although a lot of data of ²³⁷Np MB spectroscopic studies on the Np compounds have been reported, investigation for paramagnetic relaxation phenomenon is still insufficient.

This study focuses not only on the inorganic structural chemistry of actinide science, but also on the nuclear waste management. We carried out a systematic investigation on some novel neptunyl(VI) compounds by ²³⁷Np MBS, in combination with XRD, thermogravimetric (TG) analysis and magnetic susceptibility measurement.

8.1. Neptunyl(VI) Trinitrato Complex, M[NpO₂(NO₃)₃] (M = NH₄⁺, K⁺) [21]

In this study, the results indicate that the magnetic hyperfine splitting of NH₄, K and Rb salts observed in their ²³⁷Np MB spectra are due to slow paramagnetic relaxation. The δ and e^2qQ values of NH₄, K and Rb salts are the same within the experimental error. The Rietveld analyses indicate that the mean Np-O bond distances of NH₄, K and Rb salts are very close to one another. The relationship between the mean Np-O bond distance and the δ of ²³⁷Np value has been re-confirmed to the neptunyl(VI) compound. These studies suggest that the environment around Np(VI) in NH₄, K and Rb salts are similar to each other and the influence of the different M cation is relatively small for the neptunyl(VI) trinitrato complexes.

NH₄ and K salts were prepared as follows: firstly, the neptunyl(VI) nitrate salt, NpO₂(NO₃)₂·xH₂O, was prepared by adding concentrated nitric acid into a 0.1 M Np(V and VI) stock solution and then evaporating it. Then NH₄ salt (brown precipitation) was obtained by the addition of a slight excess NH₄NO₃ to the neptunyl(VI) nitrate solution, and evaporating it at about 333 K. Subsequently, K salt and freshly prepared Rb Salt were also obtained by the same method by using KNO₃ and RbNO₃, respectively.

Freshly prepared NH₄, K and Rb salts were identified by XRD. Their crystal structures were refined by RIETAN-97 β , which was based on the Rietveld method. A magnetization measurement of NH₄ salt was performed for a polycrystalline sample by using a SQUID magnetometer (MPMS, QD). The magnetic susceptibility measurement was made from 2 K to room temperature. Revision of the diamagnetism was not performed.

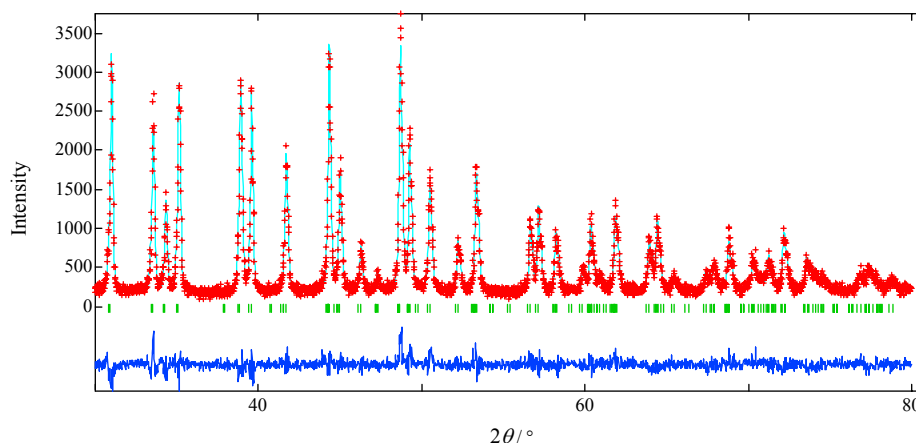


Figure 14. Result of the Rietveld refinement for NH₄[NpO₂(NO₃)₃] (Plus marks: observed, solid line: calculated; $R_{wp} = 12.67\%$, $R_p = 9.78\%$).

The result of the Rietveld refinement of NH₄ salt with space group R-3C is shown in **Figure 14**. The results suggest that different M cations can influence the lattice parameter and the unit-cell volume, but can hardly influence the bond distance and the bond angle between the Np atom and the coordinated oxygen atom. As shown in **Figure 15**, the structure of the [NpO₂(NO₃)₃]⁻ anion in NH₄, K and Rb salts adopts a hexagonal-bipyramidal

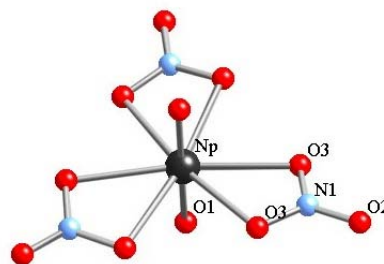


Figure 15. Structure of the [NpO₂(NO₃)₃]⁻ anion in the neptunyl(VI) trinitrato complexes.

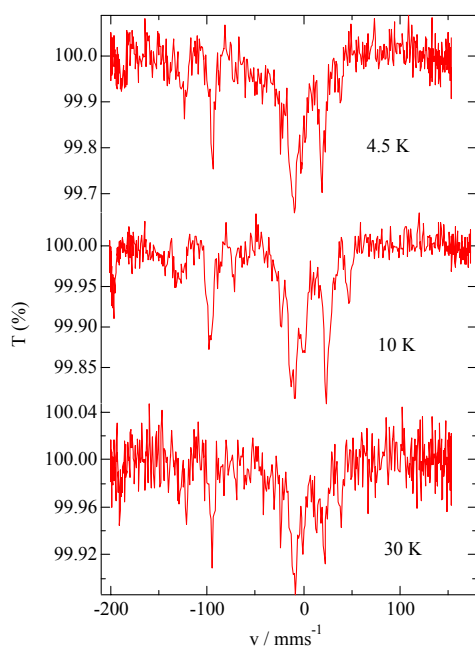


Figure 16. ^{237}Np Mössbauer spectra for $\text{K}[\text{NpO}_2(\text{NO}_3)_3]$ at 4.5, 10 and 30 K.

and two oxide ions. The mean Np-O bond-distances of NH_4 and K salts are 228.5 pm and 228.3 pm, respectively. They are very close to that of the reported Rb salt (228.4 pm) within the experimental error.

The ^{237}Np MB spectra of K salt at 4.5, 10, and 30 K are shown in **Figure 16**.

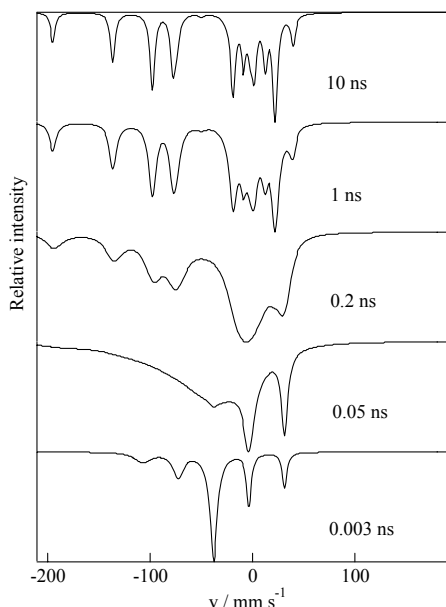


Figure 18. Simulated ^{237}Np Mössbauer spectra for several τ with $H_{\text{eff}} = 290$ T, $2\Gamma = 5$ mm s $^{-1}$, $\delta = -38$ mm s $^{-1}$ and $e^2qQ = 230$ mm s $^{-1}$. ($H_{\text{eff}} // V_{zz}$)

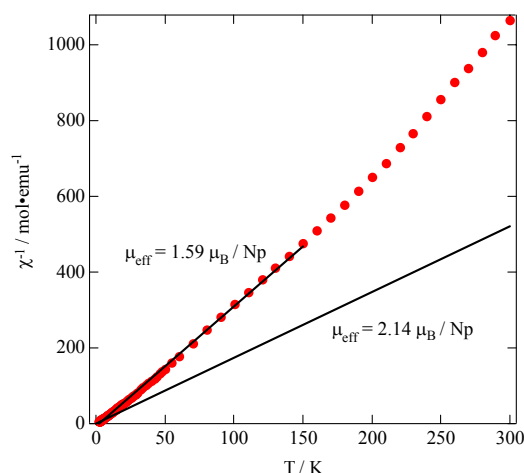


Figure 17. Plot of the reciprocal molar susceptibility against temperature for $\text{NH}_4[\text{NpO}_2(\text{NO}_3)_3]$ (Experimental: $\mu_{\text{eff}} = 1.59 \mu_B / \text{Np}$, theoretical: $\mu_{\text{eff}} = 2.14 \mu_B / \text{Np}$)

geometry consisting of the Np(VI) ion coordinated with three bidentate nitrate ions

Magnetic hyperfine splitting can be clearly observed from 4.5 to 30 K. Although neptunyl(V and VI) complexes are thought to be paramagnetic in ordinary, a ferromagnetic neptunyl(V) formate complex, $\text{NpO}_2(\text{OOCH}) \cdot \text{H}_2\text{O}$, was recently discovered below 12 K. The magnetic hyperfine splitting in the MB spectra of NH_4 , K and Rb salts may arise from two possibilities: one is slow paramagnetic relaxation, the other one is the presence of a magnetically ordered state in the measured temperature range. It is not easy to distinguish the two possibilities by only using the results of their ^{237}Np MBS.

The magnetization of NH_4 salt measured

by SQUID gives useful information about distinguishing the two possibilities. A plot of the reciprocal molar susceptibility of NH_4 salt against the temperature is shown in **Figure 17**. The reciprocal molar susceptibility nearly

follows the Curie-Weiss law from 2 K to room temperature. The value of the effective magnetic moment (μ_{eff}) was estimated to be $\sim 1.59 \mu_B / \text{Np}$, which was smaller than the theoretical value ($2.14 \mu_B / \text{Np}$) of $\text{Np}^{6+}(5f^1)$.

These SQUID data and the ^{237}Np MB spectra indicate that NH_4 salt is paramagnetic down to 2 K. The magnetic hyperfine splitting observed in NH_4 , K and Rb salt's MB spectra are due to slow paramagnetic relaxation. **Figure 18** is shown some simulated ^{237}Np MB spectra for several τ with $H_{eff} = 290 \text{ T}$, $2\Gamma = 5 \text{ mm s}^{-1}$, $\delta = -38 \text{ mm s}^{-1}$ and $e^2qQ = 230 \text{ mm s}^{-1}$, being based on the paramagnetic relaxation model. According to the simulated spectra, the ^{237}Np MB spectra of NH_4 , K and Rb salts are similar to the modulation that the τ are longer than about 1 ns. The simulation also insists that the magnetic hyperfine splitting is due to slow paramagnetic relaxation.

The δ and e^2qQ values of NH_4 , K and Rb salts are the same within the experimental error, respectively. The δ values are typical for Np(VI) compounds. We know, there is a linear relationship between the δ value and the mean Np-O bond distance for the Np(VI) compounds. In this study, almost the same Np-O bond distances of NH_4 , K and Rb salts have almost the same δ values. This is consistent with the linear relationship between the δ values and the mean Np-O bond distances established for the neptunyl(VI) compounds.

8.2. ^{237}Np MS Spectroscopic Studies on Neptunyl(VI) Oxalate and Hydroxide [22-24]

In recent years, Krot and his co-workers have reported continuously some new neptunium compounds, especially for the seven- and oxygen-coordinated neptunyl(VI) complexes as $\text{NpO}_2\text{C}_2\text{O}_4 \cdot 3\text{H}_2\text{O}$. This shows much room for the ^{237}Np MB spectroscopic study. Here, ^{237}Np MB spectra for $\text{NpO}_2\text{C}_2\text{O}_4 \cdot 3\text{H}_2\text{O}$ and an amorphous neptunyl(VI) hydroxide, $\text{NpO}_2(\text{OH})_2 \cdot x\text{H}_2\text{O}$, prepared by NaBrO_3 oxidation are discussed.

$\text{NpO}_2\text{C}_2\text{O}_4 \cdot 3\text{H}_2\text{O}$ was prepared as follows: into a small amount of Np(VI) stock solution, an excess amount of LiOH at 343 K was added until a dark brown precipitate of neptunyl(VI) hydroxide was obtained. The precipitate was separated, washed by distilled water and dried at room temperature. The dried precipitate was re-dissolved into concentrated HNO_3 . 7% $\text{H}_2\text{C}_2\text{O}_4$ solution was dropped into the freshly prepared Np(VI) nitrate solution until a grayish green crystalline, $\text{NpO}_2\text{C}_2\text{O}_4 \cdot 3\text{H}_2\text{O}$, was obtained. The grayish green crystalline was separated quickly, washed by 0.2 N HNO_3 , alcohol and ether.

Amorphous neptunyl(VI) hydroxide, $\text{NpO}_2(\text{OH})_2 \cdot x\text{H}_2\text{O}$, was prepared by the following procedure: firstly, Np(VI) stock solution was reduced into Np(V) solution by adding H_2O_2 . A neptunyl(V) hydroxide precipitate was obtained after an excess amount of NaOH was added to the Np(V) solution. The neptunyl(V) hydroxide was re-dissolved into concentrated HNO_3 . The obtained Np(V) nitrate solution was oxidized into freshly Np(VI) solution by adding NaBrO_3 . Amorphous neptunyl(VI) hydroxide, $\text{NpO}_2(\text{OH})_2 \cdot x\text{H}_2\text{O}$, was obtained by adding NH_4OH to the freshly prepared Np(VI) solution.

The oxalate and the hydroxide were examined by XRD. Thermal behavior of the hydroxide was investigated in a dry atmosphere on a Sartorius MP8 electric microbalance by recording the TG curve. The ^{237}Np MB spectra for the oxalate were computer-fitted by the relaxation procedure. The H_{eff} value was assumed as 300 T and the 2Γ was fixed to 8 mm s^{-1} . The ^{237}Np MB spectra for the hydroxide were computer-fitted by using the sum-of-Lorentzian

approximation. Values of the magnetic moments related to the ^{237}Np MB transition, used for the fitting procedure are $\mu_g = 2.8 \times 10^{-28} \text{ m}^2$ for the ground state and $\mu_e = 1.5 \times 10^{-28} \text{ m}^2$ for the excited state.

The XRD patterns indicate that the oxalate sample is pure and iso-structural with $\text{U(VI)O}_2\text{C}_2\text{O}_4 \cdot 3\text{H}_2\text{O}$.

$\text{U(VI)O}_2\text{C}_2\text{O}_4 \cdot 3\text{H}_2\text{O}$ is a seven-coordinated complex and the oxalate groups are tetradentate, each bridging two uranyl(VI) ions. Only one water molecule is coordinated with the U atom. In order to obtain the pure oxalate sample, the final grayish green crystalline must be

separated quickly. If not, some Np(VI) ions will be reduced by $\text{H}_2\text{C}_2\text{O}_4$, some bright green precipitate will be observed in the solution. However, solid state of the neptunyl(VI) oxalate is stable within three weeks though it has been reported that even in the cold the neptunyl(VI) oxalate gradually decomposed as a result of intermolecular reduction of the Np(VI) ions. This was demonstrated by the XRD patterns of our oxalate sample before and after three weeks.

The XRD patterns indicate that the hydroxide is non-crystalline phase and clearly different to the other four kinds of neptunyl(VI) hydroxides prepared in this study. Since the loss of the weight is more than one water molecular when an accurately weighted sample was heated at 100°C for 4 h, the amorphous neptunyl(VI) hydroxide is written as $\text{NpO}_2(\text{OH})_2 \cdot x\text{H}_2\text{O}$.

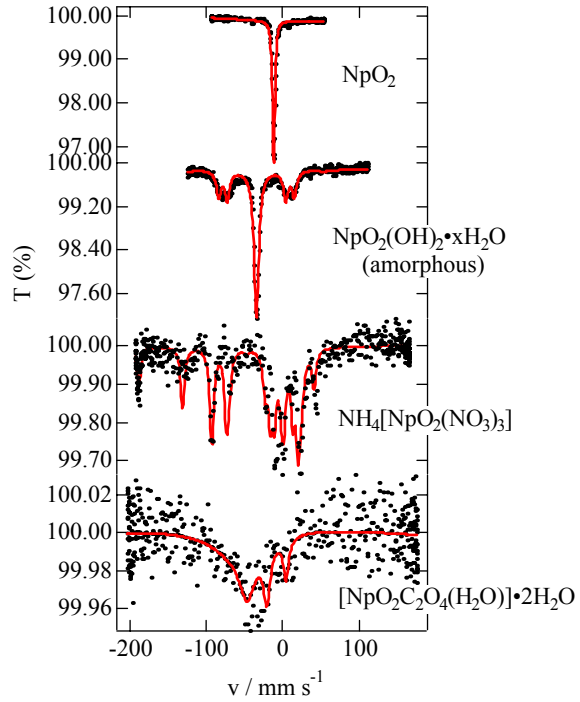


Figure 19. ^{237}Np Mössbauer spectra for several Np compounds at 10 K.

Table 3 ^{237}Np Mössbauer parameters of some Np compounds.

Compound	$\delta(\text{NpAl}_2)$ mm s^{-1}	e^2qQ mm s^{-1}	2Γ mm s^{-1}	H_{eff} T	T K
NpO_2	-6.1(4)		2.8(5)		10
$\text{NpO}_2(\text{OH})_2 \cdot x\text{H}_2\text{O}$ (amorphous)	-43.7(5)	177(1)	7.4(7)		10
$[\text{NpO}_2\text{C}_2\text{O}_4(\text{H}_2\text{O})] \cdot 2\text{H}_2\text{O}^*$	-46.8(5)	174(3)	8	300	10
$\text{NH}_4[\text{NpO}_2(\text{NO}_3)_3]$	-36.5(1)	243(1)	4.8(8)	288(1)	10
$\text{NpO}_2(\text{OH})_2$	-46.2(1)	193(1)			4.8
$\text{NpO}_2(\text{OH})_2 \cdot \text{H}_2\text{O}$ (orthorhombic)	-39.9(1)	179(1)			11
$\text{NpO}_2(\text{OH})_2 \cdot \text{H}_2\text{O}$ (hexagonal)	-43.4(1)	149(1)			11
$\text{NpO}_2(\text{OH})_2 \cdot x\text{H}_2\text{O} \cdot y\text{NH}_3$ ($x+y = 1$)	-44.6(1)	168(1)			4.6

*The values of H_{eff} and 2Γ were fixed to 300 T and 8 mm s^{-1} , respectively.

Figure 19 shows the the oxalate and the amorphous hydroxide at 10 K. For a comparison, ^{237}Np MB spectra of a standard absorber of NpO_2 and prepared $\text{NH}_4[\text{NpO}_2(\text{NO}_3)_3]$ at 10 K are also shown in **Figure 19**. Their ^{237}Np MB parameters were listed in **Table 3**. The absorption shape of NpO_2 show a symmetrical single line since NpO_2 has the cubic fluorite structure, no electric quadrupole splitting and magnetic hyperfine splitting can be observed. $\text{NH}_4[\text{NpO}_2(\text{NO}_3)_3]$ show a complex patterns due to electric quadrupole interactions and slow paramagnetic relaxation. However, the oxalate at 10 K shows broad paramagnetic relaxation pattern and the τ is clearly shorter than that of $\text{NH}_4[\text{NpO}_2(\text{NO}_3)_3]$. The hydroxide shows a pure electric quadrupole splitting patterns as well as that of the other four kinds of neptunyl(VI) hydroxides prepared in this study and no Np(V) species was observed. Since a Np(V) species was observed in the spectrum of a neptunyl(VI) hydroxide prepared by ozone oxidation, NaBrO_3 was thought to be better than ozone as a reducing agent.

The δ values of the oxalate and the hydroxide were estimated as $-46.8(3)$ and $-43.7(3)$ mm s^{-1} , respectively. These are in the characteristic range for the Np(VI) species. **Figure 20** shows the correlation between the δ and the C.N. for Np(VI) compounds. The δ value of the oxalate falls down in the reported δ range of the Np(VI) seven-coordinated

Figure 21. Plot of isomer shift (δ) against the mean Np-O bond distance for the oxygen-coordinated Np(VI) compounds. The mean Np-O bond distances may be deduced from iso-structural U(VI) compounds by using the relation: $\Delta R_{\text{U}^{\text{VI}} - \text{R}_{\text{Np}^{\text{VI}}} = 0.01$ nm, where R is the ionic radius of the six-coordinated ion.
 1: $\text{Ba}_2\text{CoNpO}_6$, 2: Li_4NpO_5 , 3: K_2NpO_4 , 4: $\beta\text{-Na}_2\text{NpO}_4$, 5: BaNpO_4 , 6: $\text{NpO}_2(\text{NO}_3)_2 \cdot x\text{H}_2\text{O}$, 7: $\text{NaNpO}_2(\text{CH}_3\text{COO})_3$, 8: $\text{Rb}[\text{NpO}_2(\text{NO}_3)_3]$, 9: NpO_2CO_3 .

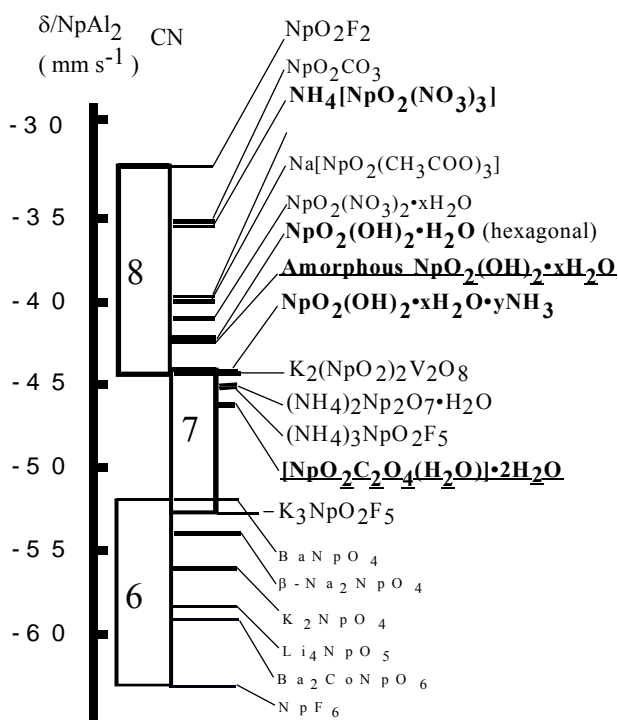
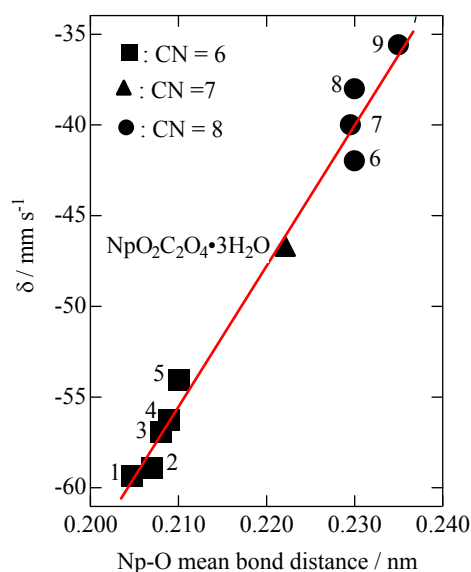


Figure 20. Plot of isomer shift (δ) against coordination number of Np for the Np(VI) compounds. The data in bold are from this study.



compounds. It is consistent with the result of the XRD analysis. The δ value of the hydroxide falls down in the reported overlap δ range of the Np(VI) seven- and eight-coordinated compounds. Comparing the results of $\text{NpO}_2(\text{OH})_2 \cdot \text{H}_2\text{O}$ (orthorhombic), $\text{NpO}_2(\text{OH})_2 \cdot \text{H}_2\text{O}$ (hexagonal) and $\text{NpO}_2(\text{OH})_2 \cdot x\text{H}_2\text{O} \cdot y\text{NH}_3$, the amorphous hydroxide is probably a eight-coordinated compound. **Figure 21** shows the plot of the δ value against the mean Np-O bond distance for the oxygen-coordinated Np(VI) compounds including the data of the oxalate. The mean Np-O bond distance of the oxalate was deduced from $\text{U(VI)O}_2\text{C}_2\text{O}_4 \cdot 3\text{H}_2\text{O}$ by using the relation: $\Delta(R_U^{VI} - R_{Np}^{VI}) = 0.01$ nm, where R was the ionic radius of the hexa-coordinated ion. The δ value of the oxalate is located between the six- and eight-coordinated Np(VI) compounds and the linear correlation between the δ value and the mean Np-O bond distance is confirmed to the six-, seven- and eight- coordinated Np(VI) compounds. Mean Np-O bond distance of the hydroxide is estimated as $\text{Np-O} \approx 0.225$ nm from **Figure 21**. The e^2qQ values of the oxalate and the amorphous hydroxide were estimated as $174(3)$ mm s^{-1} and $177(1)$ mm s^{-1} , respectively. It is the same degree with that of the other four kinds of neptunyl(VI) hydroxides prepared in this study, but clearly smaller than that of $\text{NH}_4[\text{NpO}_2(\text{NO}_3)_3]$. The τ of the oxalate was estimated as about 0.02 ns.

5. Summary

As reported above, abundant information on the coordination structure and chemical bonding in Ln and An compounds is available to be obtained from ^{155}Gd , ^{166}Er and ^{237}Np MBS in connection with other analysis technologies. Based on the reported results of the electronic structure calculations, a large quantity of ^{155}Gd MB experiment results have pointed out deeply that a small covalent contribution exists in the Ln-O (or N) bonds of various Ln(III) metal complexes and the covalent bonding is not only possible to be related to their $5d$ and $4f$ orbits but also to their $6s$ ($6p$) orbits; the covalent contribution in the Ln-O (or N) bonds should be through oxygen and/or nitrogen atoms of ligand group donating electrons to $5d$, $4f$ and $6s$ ($6p$) orbits of Gd(III) ions. ^{166}Er spectroscopic studies on Er(III) paramagnetic compounds should also suggest that there is a small covalent contribution in their Er-O (or N) bonds since the results indicate that the relaxation time is related to not only the coordination structure and spin-spin distance but also the electronic configuration.

Certainly, comparing with the participation of the $5f$ orbit in chemical bonding, the contribution of the $4f$ orbit in chemical bonding is very few. This viewpoint is available to be confirmed from all of the ^{155}Gd , ^{166}Er and ^{237}Np MB parameters obtained in this study. In the case of ^{237}Np MBS, the δ and e^2qQ values are spread out in a large range and very sensitive to the variation of the oxidation state, coordination structure and the distance between the Np atom and the nearest coordinating atom. However, the ^{155}Gd , ^{166}Er and ^{151}Eu MB parameters are only spread out in a narrow range though a tendency that the δ values of ^{155}Gd decrease with the increase in the coordination number and the nitrogen atoms coordinating to Gd(III) has been confirmed in our study. The difference should not only originate from their different mean-square nuclear radius $\Delta\langle r^2 \rangle$ and their different magnitude of quadrupole moment, Q .

Furthermore, the difference features on the coordination structure are also clearly observed from ^{155}Gd , ^{166}Er and ^{237}Np MBS between the Ln and An compounds. Since the

participation of the $4f$ orbit in chemical bonding is very few, the coordination structure in Ln compounds can be approximately considered as a closest packed structure. This means that the ligand is available to be coordinated to Ln(III) ion in all directions if some spaces are still unoccupied around the Ln(III) ion. This structural feature should be only able to cause a small electric field gradient (EFG) in the Ln nucleus position in the Ln compound, as observed from ^{155}Gd , ^{166}Er and ^{151}Eu MBS. However, in the case of the An compounds, since the participation of the $5f$ orbit in chemical bonding is large, the covalent contribution in ions like AnO_2^+ and AnO_2^{2+} become greater. As a result, all ligands are only possible to be coordinated to An in the nearly perpendicular direction to linear $(\text{O-An-O})^+$ or $(\text{O-An-O})^{2+}$ ions. This structural feature should be the main reason why there is a large EFG existing in the Np nucleus position in the Np(V and VI) compound, as observed from ^{237}Np MBS.

This study was finished when the author was at Toho University as a doctoral student and at Japan Atomic Energy Research Institute (JAERI) as a joint researcher.

References

1. S. A. Cotton, “*Lanthanide and Actinide Chemistry*”, John Wiley & Sons (2006).
2. H. Nakamatsu, T. Mukoyama, and H. Adachi, “Ionic and Covalent bonds in CeO_2 Crystal”, *Chem. Phys. Lett.* 247 (1995) 168.
3. <http://www.mossbauer.org>
4. J. Wang, “*Mössbauer Spectroscopic Studies on Gadolinium, Erbium and Neptunium Compounds*”, Doctoral Dissertation, Toho University, 2002 (in Japanese).
5. G. Czjzek, “Mössbauer Spectroscopy of New Materials Containing Gadolinium” in *Mössbauer Spectroscopy Applied to Magnetism and Materials Science*, G. J. Long and F. Grandjean (Eds), Plenum Press, New York, 1993, Vol. 1, p.373.
6. J. Stöhr and J. D. Cashion, “ ^{160}Dy and ^{166}Er Mössbauer Studies of Concentrated and Diluted Rare-Earth Dihydrides: Single-Line Compounds and Crystal-Field Effects”, *Phys. Rev. B* 12 (1975) 4805.
7. J. Jove, L. He, J. Proust, M. Pages, and P. Pykkö, “Mössbauer Spectroscopy as a Nuclear Probe for Solid State Transuranium Chemistry”, *J. Alloys Comp.* 177 (1991) 285.
8. J. Wang, M. Takeda, and T. Shishido, “Development and Evaluation of a New $^{155}\text{Eu}/^{154}\text{SmPd}_3$ Source for Use with ^{155}Gd Mössbauer Spectroscopy”, *J. Nucl. Mater.* 340 (2005) 52.
9. J. Wang, M. Takahashi, and M. Takeda, “Crystal Structures and ^{166}Er Mössbauer Spectra of Some Er(III)- β -diketonato Complexes”, *Bull. Chem. Soc. Jpn.* 75 (2002) 735.
10. M. Nakada, M. Saeki, N. M. Masaki, and S. Tsutsui, “Preparation of source and sealed absorber holder for ^{237}Np and ^{238}U Mössbauer measurements”, *J. Radioanal. Nucl. Chem.*, 232 (1998) 201.
11. J. Wang, “Structure and Bonding in Some Gd(III) Metal Complexes Studied by

- Three-Dimensional X-Ray Analysis and ^{155}Gd Mössbauer Spectroscopy”, to be published.
12. J. Wang, M. Takahashi, T. Kitazawa, and M. Takeda, “ ^{155}Gd Mössbauer Spectra of Some Gd(III)- β -Diketonato Complexes”, *J. Radioanal. Nucl. Chem.* 255 (2003) 195.
 13. J. Wang, J. Abe, T. Kitazawa, M. Takahashi, and M. Takeda, “ ^{155}Gd Mössbauer Spectroscopic Study of $\text{GdM}(\text{CN})_6 \cdot 4\text{H}_2\text{O}$ ($\text{M} = \text{Cr}^{\text{III}}$, Fe^{III} and Co^{III}) and $\text{KGdM}(\text{CN})_6 \cdot 3\text{H}_2\text{O}$ ($\text{M} = \text{Fe}^{\text{II}}$ and Ru^{II})”, *Z. Naturforsch.* 57a (2002) 581.
 14. M. Takeda, J. Wang, T. Nishimura, K. Suzuki, T. Kitazawa, and M. Takahashi, “ ^{155}Gd Mössbauer Isomer Shifts and Quadrupole Coupling Constants of Gadolinium Complexes”, *Hyperfine Interactions*, 156-157 (2004) 359.
 15. J. Wang, M. Takeda, and A. Nakamura, “Influence on the Structural Characteristics of Defect solid Solution $\text{Gd}_x\text{Zr}_{1-x}\text{O}_{2-x/2}$ with $0.18 \leq x \leq 0.62$ under Longer Term Annealing Studied by ^{155}Gd Mössbauer Spectroscopy”, *J. Nucl. Mater.* 340 (2005) 33.
 16. J. Wang, A. Nakamura, and M. Takeda, “Structural Properties of the Fluorite- and Pyrochlore-Type Compounds in the Gd_2O_3 - ZrO_2 System $x\text{GdO}_{1.5}-(1-x)\text{ZrO}_2$ with $0.18 \leq x \leq 0.62$ ”, *Solid State Ionics* 164 (2003) 185.
 17. J. Wang, H. Otobe, A. Nakamura, and M. Takeda, “Correlation of Crystal Structures with Electric Field Gradients in the Fluorite- and Pyrochlore-Type Compounds in the Gd_2O_3 - ZrO_2 System”, *J. Solid State Chem.* 176 (2003) 105.
 18. A. Nakamura, H. Otobe, J. Wang, and M. Takeda, “ ^{155}Gd Mössbauer Spectroscopic and X-ray Diffraction Study of the $\text{Zr}_{1-x}\text{Gd}_x\text{O}_{2-x/2}$ ($0 < x \leq 1.0$) System”, *J. Phys. Chem. Solids* 66 (2005) 356.
 19. M. Takeda, J. Wang, M. Takahashi, T. Shishido, A. Yoshikawa, and A. Nakamura, “ ^{166}Er and ^{155}Gd Mössbauer Spectroscopy of R-Rh-B ($\text{R} = \text{Er}, \text{Gd}$) System”, *J. Alloys and Compounds* 408-412 (2006) 371.
 20. J. Wang, “Structural Characterization of the $\text{Gd}_x\text{Zr}_{1-x}\text{O}_{2-x/2}$ System by ^{155}Gd Mössbauer Spectroscopic Study” Chapter 8 in *Nuclear Materials Research Developments*, J. E. Keister (Ed), Nova Science Publishers (ISBN:1-60021-432-0), New York, 2006, in press.
 21. J. Wang, T. Kitazawa, M. Nakada, T. Yamashita, and M. Takeda, “Structural Characterization of Neptunyl(VI) Trinitrato Complexes: $\text{M}[\text{NpO}_2(\text{NO}_3)_3]$ ($\text{M} = \text{NH}_4^+$ and K^+)”, *Bull. Chem. Soc. Jpn.* 75 (2002) 253.
 22. J. Wang, T. Kitazawa, M. Nakada, T. Yamashita, and M. Takeda, “ ^{237}Np Mössbauer Spectra for Neptunyl(VI) Oxalate $\text{NpO}_2\text{C}_2\text{O}_4 \cdot 3\text{H}_2\text{O}$ and Amorphous Neptunyl(VI) Hydroxide $\text{NpO}_2(\text{OH})_2 \cdot x\text{H}_2\text{O}$ ”, *J. Nucl. Sci. Technol.* Suppl. 3 (2002) 429.
 23. T. Saito, J. Wang, T. Kitazawa, M. Takahashi, M. Takeda, M. Nakada, T. Nakamoto, N. M. Masaki, T. Yamashita, and M. Saeki, “Synthesis of Neptunyl(VI) Hydroxides and Their ^{237}Np Mössbauer Spectra”, *J. Radioanal. Nucl. Chem.* 239 (1999) 319.
 24. M. Nakada, T. Kitazawa, T. Saito, J. Wang, M. Takeda, T. Yamashita, and M. Saeki, “A New Type of Neptunyl(VI) Hydroxide which is Topologically Similar to $\alpha\text{-UO}_2(\text{OH})_2$ ”, *Bull. Chem. Soc. Jpn.* 76 (2003) 1375.